

Description of new diplomonads (Diplomonada, Euglenozoa) and their endosymbionts: Charting the morphological diversity of these poorly known heterotrophic flagellates

Daria Tashyreva^{a,*}, Jan Votýpka^{b,c}, Akinori Yabuki^{d,e}, Aleš Horák^{b,f}, Julius Lukeš^{b,f,*}

^a Institute of Evolutionary Biology, Faculty of Biology, University of Warsaw, Warsaw, Poland

^b Institute of Parasitology, Biology Centre, Czech Academy of Sciences, České Budějovice, Czech Republic

^c Faculty of Sciences, Charles University, Prague, Czech Republic

^d Japanese Agency for Marine-Earth Science and Technology, Yokosuka, Japan

^e Advanced Institute for Marine Ecosystem Change (WPI-AIMEC), Yokohama, Kanagawa 236-0001, Japan

^f Faculty of Science, University of South Bohemia, České Budějovice, Czech Republic

ARTICLE INFO

Keywords:

Endosymbiont

Ultrastructure

Flagellate

Lacrimia

Rhynchopus

Chlamydiae

Heterotrophic protist

Intracellular bacteria

ABSTRACT

Diplomonads are a hyperdiverse group of flagellated protists, but with less than two dozen formally described representatives. Here, we describe four new species of cultured diplomonads, identified on the basis of their 18S rRNA sequences, light-, fluorescence-, scanning- and transmission electron microscopy. Three new species belong to the genus *Rhynchopus* (*R. asiaticus* sp.n., *R. granulatus* sp.n., and *R. valaseki* sp.n.), while the fourth species is an unusual representative of the genus *Lacrimia* (*L. aflagellata* sp.n.). The latter organism is the first diplomonad outside the genus *Rhynchopus* (as defined previously) to show a gliding trophic stage with flagellar stubs concealed inside the flagellar pocket and a highly motile dispersive swimming stage. Since this character is thus no longer a genus-specific apomorphy, we provide a taxonomic revision of the genus *Rhynchopus* with separation of the new genus *Natarhynchopus* gen. n. We also identify bacterial endosymbionts of *L. aflagellata* and *R. asiaticus* as *Ca. Syngnamydia* medusae (*Chlamydiales*, *Simkaniaceae*) and *Ca. Cytochromobacter rhynchopi* sp. n. (*Alphaproteobacteria*, *Holospiraceae*), respectively, and discuss their potential functions. This is the first report of a chlamydial symbiont within a diplomonad host. We also propose that diplomonads may serve as vectors for chlamydial pathogens of marine fish.

1. Introduction

It is now widely accepted that heterotrophic flagellates are very prominent among protists in terms of genomic, functional, and evolutionary diversity (Lukeš et al., 2024). This is particularly true for marine diplomonads (Diplomonada, Euglenozoa), which are still considered among the least understood microorganisms despite their presumed major ecological and evolutionary importance (Tashyreva et al., 2022). Some diplomonad groups, such as Eupelagonemidae, appear to be ubiquitous in the world's oceans, as they are abundant in both the sunlit zone (de Vargas et al., 2015), deep waters (Okamoto et al., 2019), deep-sea mud (Cadena et al., 2024), and are distributed in both the equatorial zones as well as the Antarctic (Flegontova et al., 2020). While environmental sequencing suggests that diplomonads belong to one of the

most diverse eukaryotic groups (Flegontova et al., 2016; Gawryluk et al., 2016), with the latest estimates reaching thousands to tens of thousands of species (Flegontova et al., 2020), the number of morphologically described species and those present in axenic cultures can essentially be counted on our fingers (Tashyreva et al., 2022). This enormous estimated diversity has been questioned due to over-interpretation of sequence differences and possible intra-genomic variability of the widely used V9 domain for their 18S rRNA genes (Mukherjee et al., 2019). However, a detailed comparative analysis showed that the intra-genomic rRNA diversity of diplomonads does not exceed that of other eukaryotes (Flegontova et al., 2023), and hence, at least from this perspective, their predicted richness is valid.

The rather sparse literature on the morphology and taxonomy of diplomonads has been partially influenced by their inconspicuous

* Corresponding authors at: Institute of Evolutionary Biology, Faculty of Biology, University of Warsaw, Warsaw, Poland (D. Tashyreva); Institute of Parasitology, Biology Centre, Czech Academy of Sciences, České Budějovice, Czech Republic (J. Lukeš).

E-mail addresses: d.tashyreva@uw.edu.pl (D. Tashyreva), jula@paru.cas.cz (J. Lukeš).

<https://doi.org/10.1016/j.protis.2025.126090>

Received 9 May 2024; Accepted 17 February 2025

Available online 20 February 2025

1434-4610/© 2025 Published by Elsevier GmbH.

morphology and the failure to introduce representatives of the most species-rich clade Eupelagonemidae into culture. However, the recent establishment of a high-quality genome and transcriptome for the model species *Paradiplonema papillatum* (Valach et al., 2023a), which can additionally be genetically manipulated (Faktorová et al., 2020a), brings diplomonids into the still narrow group of marine protists amenable to functional genomics (Faktorová et al., 2020b). Indeed, the ability to tag proteins and identify their interacting partners allowed the characterization of an extremely rRNA-poor and complex mitochondrial ribosome of *P. papillatum* (Valach et al., 2023b), the initial characterization of its membrane trafficking system (Faktorová et al., 2023), and the description of highly unorthodox kinetochores (Benz et al., 2024). Although only a few species have been studied so far, diplomonids have turned out to be anything but mundane. They harbor a novel, morphologically striking membranous organelle involved in trafficking of vesicles derived from the feeding apparatus (Tashyreva et al., 2023), are capable of the most efficient accumulation of strontium documented so far (Pílatová et al., 2023), have evolved the most extreme forms of RNA editing in their mitochondrion (Kaur et al., 2020), and frequently harbor a range of endosymbiotic bacteria (George et al., 2020), to name just the most prominent aspects of their known biology.

Until recently, only a few diplomonid species belonging to the genera *Diplonema*, *Hemistasia* and *Rhynchopus* had been described (Tashyreva et al., 2018b). This has now changed and the morphologically known diversity of these heterotrophic biflagellates, complemented by 18S rRNA-based phylogeny, has been extended to the genera *Paradiplonema*, *Metadiplonema*, *Lacrimia*, *Flectonema*, *Sulcionema* and *Eupelagonema* (Tashyreva et al., 2022; Lax et al., 2024). In this work, we have introduced into culture and characterized four new diplomonid species, two of which host bacterial endosymbionts. We also provide an update and expansion of the diplomonid taxonomy and systematics, although we acknowledge that we are still only scratching the surface of their diversity, as most of it remains hidden in the yet-to-be-cultivated eupelagonemids (Okamoto et al., 2019).

2. Materials and methods

2.1. Isolation and cultivation

Samples of seawater from Japan were collected into 1 l glass bottles and stored at 13 °C for two days. The sample from Mexico was collected into a 40 ml plastic cultivation flask and stored at room temperature for a week before cells were isolated. Information about these samples is summarized in Table 1. Axenic clonal cultures were established by picking single cells with a glass microcapillary with inverted microscopes CKX31 (Olympus) or Primovert (Zeiss) and inoculating them into Hemi medium (Tashyreva et al., 2018b) supplemented with a 10 µl/ml antibiotic cocktail (P4083, Sigma-Aldrich). The blood serum in the medium supports the growth of a wide range of diplomonids, which are

known as predators of large eukaryotes ('protoplast feeders') and opportunistic parasites of multicellular organisms (Tashyreva et al., 2022). Subsequently, all strains were maintained in antibiotic-free Hemi medium. *Rhynchopus valaseki* YZ270 cl. 9, *Rhynchopus asiaticus* YZ270 cl. 10, and *Rhynchopus granulatus* DT0508 were cultivated at 13 °C, while *Lacrimia aflagellata* Mex301 was kept at 23 °C. For nutrient starvation, which is known to induce differentiation into the swimming stage, cell pellets were resuspended in seawater lacking organic nutrients.

Table 1. Information on the origin of the isolates.

2.2. DNA isolation and sequencing

Total genomic DNA was isolated from cultures with a DNeasyBlood & Tissue Kit (Qiagen) following protocol A. Nearly full-size 18S rRNA gene sequences were PCR-amplified in triplicates with universal eukaryotic primers SA (5'-AACCTGGTTGATCCTGCCAGT-3') and SB (5'-TGATCCTCCTGCAGGTCCACCT-3') using OneTaq® 2× Master Mix with Standard Buffer (BioLabs, Cat. N. M0482L) following the manufacturer's protocol. The PCR amplification consisted of initial denaturation step at 94 °C for 3 min, followed by 35 cycles at 94 °C for 30 s, 58 °C for 30 s, and 68 °C for 2 min 20 s, and the final extension step at 68 °C for 5 min. The amplicons were purified and Sanger sequenced using primers SA, SB, and an internal primer (5'-GGTTCGATTCCGGAGAGGG-3'). A partial (1111-nt long) 16S rRNA sequence of the bacterial symbiont of *L. aflagellata* was PCR-amplified in triplicates with universal bacterial primers U337F (5'-GACTCCTACGGGAGGCWGCAG-3') and U1492R (5'-CGGTTACCTTGTACGACTT-3') and Sanger sequenced. The sequence can also be amplified with *Chlamydiae*-specific PanR as a reverse primer (5'-GTCATCRGCCYYACCTTVSRCRYTCT-3') but not U8Fdeg (5'-AGAGTTTGATYMTGGCTCAG-3'), U63F (5'-CAGGCCTAACACATGCAAGTC-3'), or PanF (5'-CGTGGATGAGGCATGCRAGTCG-3') as forward primers, which are used for amplification of nearly full-size 16S rRNA gene sequences in bacteria, evidently due to a mismatch at the primer binding site. The 16S and 18S rRNA gene sequences were de novo assembled from individual reads in Geneious Prime, with 3 to 6 coverage for 16S rRNA and 3 to 9 coverage for 18S rRNA gene.

Total genomic DNA from *R. asiaticus* and its symbiont was isolated by phenol-chloroform extraction as follows: pelleted cells (50 mg) were resuspended in 1.5 ml lysis buffer (100 mM Tris-HCl pH 8.0; 100 mM EDTA; 1.15 % polyvinylpyrrolidone; 5 mM spermidine; 0.5 % N-laurylsarcosine), treated with 0.2 mg of RNase for 30 min at 37 °C and with 100 µl proteinase K (10 mg/ml) for 60 min at 37 °C, mixed with an equal volume of phenol: chloroform: isoamyl alcohol (25:24:1) and centrifuged at 4,000g and 4 °C for 10 min. Aqueous phase was mixed with 2 volumes of ice-cold ethanolic solution of 0.5 M ammonium acetate. Precipitated DNA was removed with a glass hook, rinsed with 1 ml of pre-chilled 80 % ethanol (4 °C) and solubilized in 50 µl of 10 mM Tris-HCl pH 8.5 at 4 °C overnight. A TruSeq DNA libraries were sequenced using Illumina Novaseq 6000. Raw reads were quality treated, adapter-trimmed using Trimmomatic v.039 (Bolger et al., 2014), and the cleaned reads were assembled using SPAdes v3.15.1 with default settings and autodetection of best kmer (Prjibelski et al., 2020).

2.3. Phylogenetic analysis of diplomonids and their endosymbionts

The 18S rRNA gene sequences of four new diplomonid species described here were added to a dataset covering the known diversity of diplomonids that included 32 eupelagonemids, three hemistasiids, four members of the environmental clade DSPDII (Flegontova et al., 2016), and 34 representatives of Diplonemidae, while 9 kinetoplastid species were used as an outgroup. The whole dataset was aligned using the genafpair algorithm in Mafft v7.505 (Katoh and Standley, 2013). Ambiguous and hypervariable sites were then manually removed in SeaView 5 (Gouy et al., 2021) resulting in an alignment containing 79 taxa and 1880 positions. Sequence identity between the diplomonid species described herein (and their close relatives) was estimated using

Table 1
Information on the origin of the isolates.

| Isolate | Sample | Locality | Collection method | Sampling date |
|-------------|--|--|---------------------|---------------|
| YZ270 cl.9 | Pumped deep-sea water (270 m) | Shizuoka prefectural deep-sea water pumping facility, Yaizu, Japan | 1 l glass bottle | Mar 20, 2018 |
| YZ270 cl.10 | Pumped deep-sea water (270 m) | Shizuoka prefectural deep-sea water pumping facility, Yaizu, Japan | 1 l glass bottle | Mar 20, 2018 |
| DT0508 | Spider crab tank seawater | Enoshima aquarium, Fujisawa, Japan | 1 l glass bottle | Nov 15, 2019 |
| Mex301 | Seawater with scrapings of algal biofilm | Zoo Payo Obispo, Chetumal, Mexico | 40 ml plastic flask | Feb 22, 2022 |

the SeaView built-in distance analysis tool. To ensure correct alignment of individual sequence pairs, we put together a dataset containing only closely related species (see Suppl. Table 1) and aligned them using Mafft. Sequence identities for each individual pair were then inferred from the alignment.

The 16S rRNA gene sequence of the symbiont of *R. asiaticus* described herein as *Ca. Cytomitobacter rhynchopi* sp. n. was extracted from the genomic assembly based on Illumina Novaseq 6000 PE 150 genomic reads (see above). The preliminary blastn-based analysis suggested its affiliation to *Cytomitobacter* spp. To confirm this, the sequence was placed in the dataset covering the alpha-proteobacterial diversity with emphasis on *Holosporaceae* and *Magnetococcus marinus* used as an out-group. The dataset was processed as described above resulting in alignment containing 145 sequences and 1432 positions. 16S rDNA of symbiont of *L. aflagellata* was amplified using the oligonucleotides described above. Based on the results of blastn search and sequence similarity (99.1 %), the symbiont was identified as *Syngnamydia medusae* (Viver et al., 2017). To confirm this, we created the 16S rDNA dataset including chlamydiae of orders Chlamydiales and Parachlamydiales. The dataset was processed as described above, resulting in an alignment containing 59 sequences and 1508 positions. The 18S and 16S rRNA gene sequences obtained in this study are deposited at NCBI under the following accession numbers (PP719295, PP719297, and PP719300).

The phylogenetic placement of new diplonemids was inferred using the Maximum Likelihood under the SYM model with four free-rate categories (SYM + R4) as implemented in IQTree 2 (Minh et al., 2020). This particular model was identified as best-fitting according to both Akaike and Bayesian information criterion, as inferred by model finder implemented in IQTree 2. The branching support was estimated using the non-parametric bootstrap values inferred from 1000 replicates in IQTree 2 (–b 1000 option) as well as Bayesian posterior probabilities. The latter were inferred in Phylobayes 4.1c (Lartillot et al., 2009) with exchange rates defined by the general time-reversible model and the number of categories limited to 40 (GTR + C40 model). Four independent Markov chains were run until they converged (i.e. the maximum observed discrepancy was below 0.1 and the effective sample size of observed parameters exceeded 100) with initial 20 % of generations discarded ('burnin' parameter set to 0.2) and all trees used in estimates. The significance of observed topologies in specific cases was tested using an approximately unbiased test, as implemented in IQTree 2. The phylogenetic positions of the bacterial symbionts of *R. asiaticus* and *L. aflagellata* were estimated the same way as those of their hosts. For the former, the phylogeny was estimated using the TVMe+R6 matrix while for the latter it was GTR + F + I + I + R4 (both chosen as the best-fitting based on BIC score). All trees were visualized in SeaView 5 built-in tree viewer and edited for publication in Inkscape v1.3 (<https://inkscape.org/>). All alignments, together with corresponding IQTree run logs, the Newick-format maximum likelihood and Bayesian inference trees are available as supplemental material (Supplementary files 2–13).

2.4. Light and electron microscopy

Live cells from fresh batch cultures (2–5 days after transfer to fresh Hemi medium) and starved cultures (placed in plain seawater) were observed under Olympus BX53 or Olympus BX63 microscopes equipped with differential interference contrast and photographed or recorded with a DP72 microscope digital camera at 1600 × 1200-pixel resolution using CellSens software v. 1.11 (Olympus). Cell dimensions were measured using Image J v.53 t.

For DNA staining, immunofluorescence assay (IFA), and fluorescence in situ hybridization (FISH), cells of all strains were fixed with 4 % paraformaldehyde dissolved in seawater, except for *L. aflagellata* that was fixed with OsO₄ as previously described (Tashyreva et al., 2023). Intracellular bacteria were labeled by FISH with a universal bacterial Eub338 probe (5'-GCTGCCTCCCGTAGGAGT-3') 5'-labeled with Cy3 dye, using hybridization buffer containing 20 % formamide (v/v) as

described elsewhere (George et al., 2020). In *R. valaseki*, the mitochondrion was visualized by the IFA with rabbit polyclonal antiserum against purified ATPase complex of *Crithidia fasciculata*, used at 1:500 dilution (Maslov et al., 2002). To visualize DNA, microscopy slides were stained with DAPI (George et al., 2020). Images were taken with a Zeiss AxioPlan 2 fluorescence microscope equipped with a DP72 microscope digital camera at 1600 × 1200-pixel resolution using CellSens software v. 1.11 (Olympus) and processed in GIMP v. 2.10.14, Irfan View v. 4.54, and Image J v. 1.53 t. The dimensions of the *Rhynchopus asiaticus* symbiotic bacteria were estimated using Image J from high-resolution FISH images, which were taken at 100× magnification.

For electron microscopy, cells were harvested by centrifugation at 3000g for 10 min. Transmission electron microscopy (TEM) samples and data were processed as previously described (Tashyreva et al., 2023). During scanning electron microscopy (SEM) processing, previously published protocols were followed (Tashyreva et al., 2023), except *L. aflagellata* was fixed for 30 min with 4 % paraformaldehyde (w/v) dissolved in seawater instead of OsO₄ fixation.

3. Results

3.1. Phylogenetic analysis of diplonemids

In agreement with the preliminary results of nucleotide blast searches against the NCBI nr database, the maximum likelihood phylogeny (Fig. 1) of the dataset containing 79 taxa and 1880 sites positioned the new isolates within Diplonemidae. The topology is consistent with previously published results recognizing Diplonemidae as one of the major clades of diplonemids, together with Eupelagonemidae, Hemistiadiidae and the environmental clade DSPD II (deep-sea pelagic diplonemid clade II). Diplonemidae are further subdivided with *Sulcionema specki* and *Flectonema neradi*, branching as sister-lineages to other members of the Diplonemidae, which form three crown groups roughly corresponding to the genus *Lacrimia*, *Diplonema* as well as the recently erected *Metadiplonema* and *Paradiplonema* (Tashyreva et al., 2022) and *Rhynchopus* s.l. (including the genus *Natarhynchopus* established here). The mutual relationships between the respective diplonemid crown lineages remain unresolved, as reflected by short internal branches and lack of branching support, suggesting rapid differentiation followed by subsequent speciation.

Three new species described herein as *Rhynchopus valaseki*, *R. granulatus*, and *R. asiaticus*, together with an environmental sequence originating from microbial mats in deep-sea cold seep sediment (NCBI acc. n. AB505540), form a robustly supported clade branching as a sister to *R. euleeides*. Together with another clade of four taxa, with *R. serpens* as the only formally described species, they cover the diversity of the genus *Rhynchopus* as we define it here. Because of the high molecular divergence (~ 15 %) in the 18S rRNA gene, we decided to remove *R. humris* and *Rhynchopus* sp. SH-2004-II from the genus *Rhynchopus* and place them into the newly established genus *Natarhynchopus*. See Discussion for morphological and behavioral features distinguishing the genera *Rhynchopus* and *Natarhynchopus*.

Another novel diplonemid isolate is found nested within the genus *Lacrimia*, and therefore described as *L. aflagellata* sp. n. Due to its morphological similarity to the genus *Natarhynchopus* and the lack of branching support anchoring its position within the genus *Lacrimia*, we have decided to test the robustness of its placement using the approximately-unbiased topology test. Although we were unable to reject alternative topologies with *L. aflagellata* branching as a sister clade to other *Lacrimia* spp. (including environmental sequences present within the *Lacrimia* s.l. clade) (Fig. 1), all topologies with *L. aflagellata* branching outside the *Lacrimia* clade were rejected.

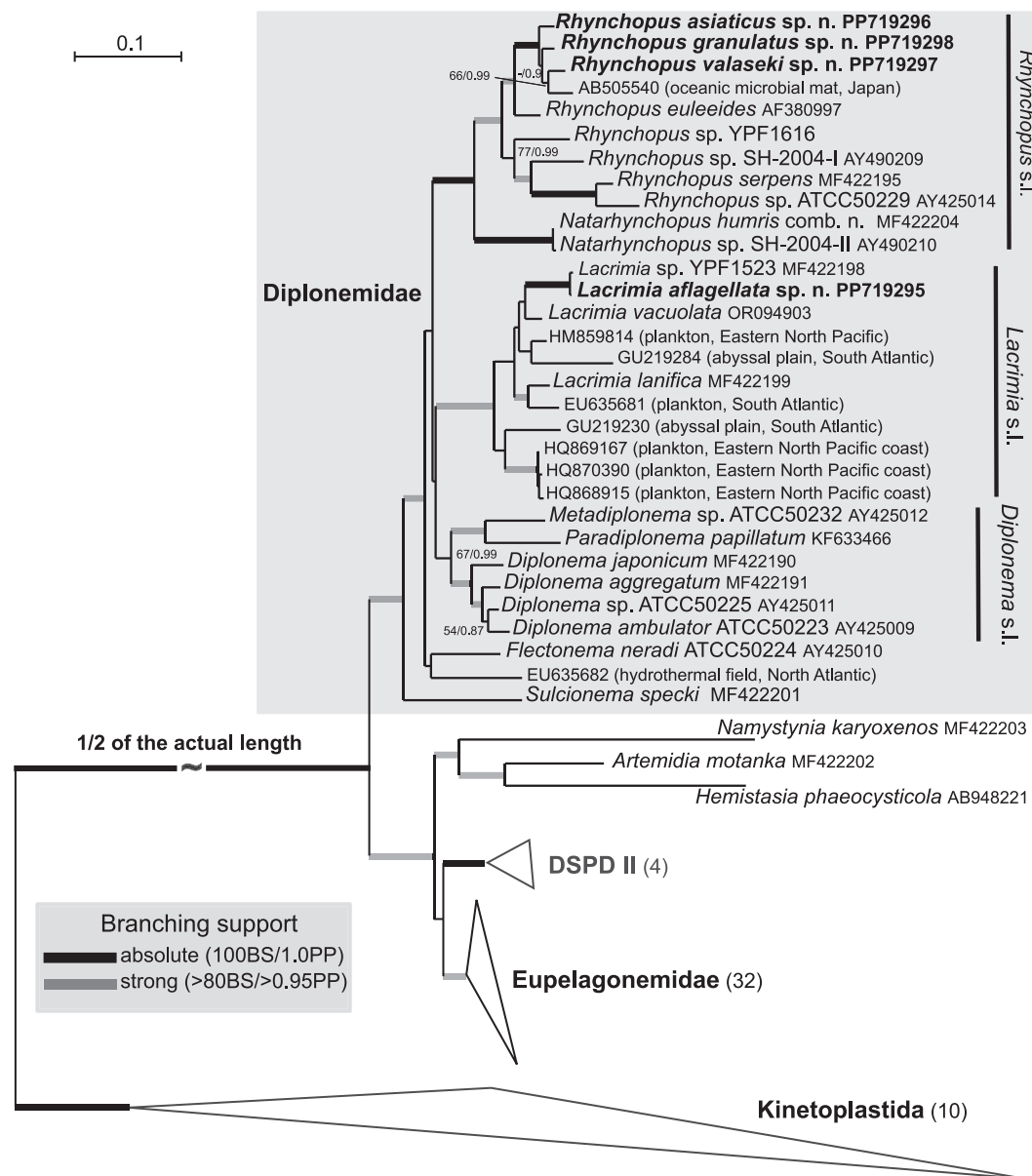


Fig. 1. 18S rDNA maximum likelihood phylogeny showing the placement of the newly described species in the context of diplonemid diversity. The tree is based on the analysis of 80 taxa and 1880 positions under the SYM + R4 model in IQTree2 (which was selected as the best fitting model using the ModelFinder implemented in IQTree2). The branching support in the form of thickened branches or numbers pointing to relevant nodes represents the non-parametric bootstrap (BS) analysis of 1000 replicates (option -b 1000) using the 'thorough' algorithm in IQTree2 as well as Bayesian posterior probabilities (PP). The latter were estimated from four MCMC chains run in Phylobayes 4.1 under the GTR + C40 model (see Methods for details). Support is shown only for nodes with BS = 80 and higher and/or PP = 0.95 and higher. For readability reasons, some clades that are not directly relevant to the species described are shown as collapsed.

3.2. Isolation and light microscopy

3.2.1. *Rhynchopus granulatus* (DT0508) sp. n

Three single cells were isolated into clonal axenic cultures four days after inoculating 100 µl of clear aquarium water into 5 ml of Hemi medium supplemented with antibiotics. In fresh cultures, these relatively large cells measured 16.3 to 28.2 µm in length (21.6 ± 6.8 µm; $N = 69$) and 4.8 to 8.7 µm in width (6.8 ± 0.8 µm; $N = 69$). Although *R. granulatus* is capable of metabolic contortions (euglenoid-type irregular deformations of the entire cell body) and slow gliding on surfaces, such behavior is rare in culture, with cells mostly motionless and uniformly suspended in the water column. Cell bodies are cylindrical, with only a slightly constricted anterior tip (Fig. 2A) associated with an apical papilla, which is barely discernable under the light microscope. A deep subapical flagellar pocket with short flagellar stubs and a rigid J-shaped

cytopharynx are poorly visible due to extensive granulation throughout the cytoplasm (Figs. 2A, B). A large rod-shaped crystal inside a vacuole is sometimes seen in the central part of the cell body (Fig. 2B). Cells in starved (nutrient-free) and old batch cultures diminish in size and reduce granulation, but do not change shape or form cysts, and never differentiate into fast-swimming cells with lengthened flagella.

3.2.2. *Rhynchopus valaseki* (YZ270 cl. 9) sp. n. and *Rhynchopus asiaticus* (YZ270 cl. 10) sp. n

Both isolates originated from a water sample pumped from a depth of 270 m. A few days after inoculation into Hemi medium, 18 clonal cell lines were established from single cells, out of which, based on the 18S rRNA gene sequences, two belonged to a new species designated as *R. valaseki*, and 16 clonal lines belonged to another named *R. asiaticus*.

Cells of *R. valaseki* are cylindrical, with a narrowed anterior and

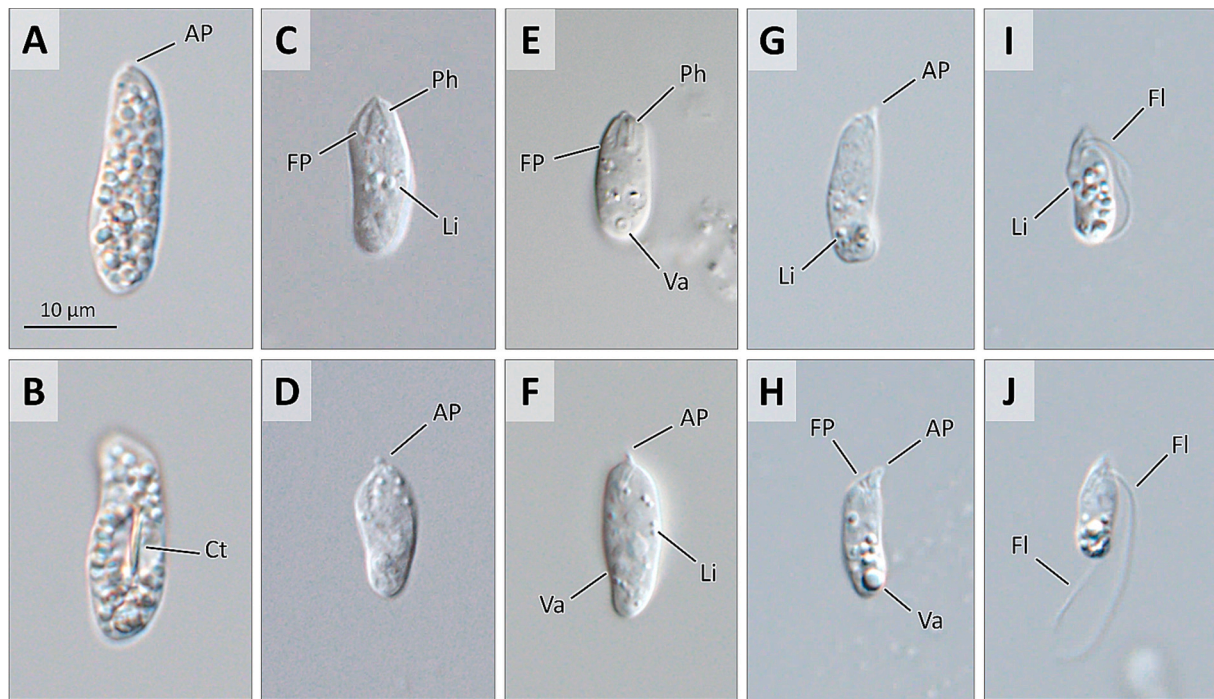


Fig. 2. Differential interference contrast micrographs of live cells of *Rhynchopus granulatus* sp. n. (A, B), *R. valaseki* sp. n. (C, D), *R. asiaticus* sp. n. (E, F), and *Lacrimia aflagellata* sp. n. (G–J) in trophic (G, H) and swimming (J) stages, and cell during transition into swimming cell (I). AP – apical papilla, Ct – crystal, Fl – flagellum, FP – flagellar pocket, Li – lipid-like inclusion, Ph – cytopharynx, Va – vacuole. Scale bar applies to all figures.

rounded posterior (Figs. 2C, D). Cytoplasmic droplets, granules, and vacuoles are scarce and, if present, are located in the posterior region of the cell. Even in fresh, nutrient-supplemented cultures, cells display notable variability in size, measuring from 7.9 to 19.9 μm in length ($12.9 \pm 2.9 \mu\text{m}$; $N = 54$) and 3.0 to 7.6 μm in width ($5.2 \pm 0.9 \mu\text{m}$; $N = 54$). This variability was absent in freshly established cultures, which were characterized by consistently larger and rather uniform cells. *R. valaseki* does not glide and exhibits metabolic movements only when compressed between a microscopic slide and a coverslip. Deep subapical flagellar pocket, cytopharynx, and apical papillae are readily seen under a light microscope (Figs. 2C, D). Starvation does not trigger differentiation of trophic cells into a swimming stage.

Cells of *R. asiaticus* are morphologically similar to those of *R. valaseki*, but larger and overall less variable in size. Cell dimensions range from 12.4 to 23.6 μm in length ($15.9 \pm 2.5 \mu\text{m}$; $N = 51$) and 3.9 to 5.9 μm in width ($5.3 \pm 0.6 \mu\text{m}$; $N = 51$). Small lipid-like inclusions and vacuoles are commonly scattered throughout the cytoplasm (Figs. 2E, F). The apical papillae, subapical flagellar pocket carrying short flagellar stubs and cytopharynx can be distinguished at a light microscopy level (Figs. 2E, F). In culture, trophic cells typically slowly glide at the bottom of culture flasks and display metabolic movement typical for diplomonads. Fast-swimming stages with long flagella are never observed in starved or old batch cultures.

3.2.3. *Lacrimia aflagellata* (Mex301) sp. n

The original sample of aquarium water with biofilm scrapings contained predominantly multicellular algae and other photosynthetic organisms, whereas diplomonad-like cells were not observed. After one week in darkness, as the algae had partially decayed, both fast-swimming and small gliding cells began to emerge. Sequencing of five clonal cell lines showed that they shared identical 18S rRNA sequences. After transfer to Hemi medium, only non-flagellated (Figs. 2I, J) and highly metabolic cells were present, which moved quickly by gliding at the bottom of the flask and frequently changed direction (Supplementary Video 1). When gliding, the posterior end of the body is turned somewhat upward at an obtuse angle relative to the substrate. In fresh,

nutrient-supplemented cultures, the cell length ranged from 10.2 to 16.7 μm ($14.1 \pm 1.5 \mu\text{m}$; $N = 60$), while the width ranged from 4.1 to 5.6 μm ($4.7 \pm 0.4 \mu\text{m}$; $N = 60$). Most of these cells showed notable cytoplasmic granulation, which was more pronounced in their posterior half (Fig. 2J). A pair of short parallel flagella were either entirely concealed inside the deep subapical flagellar pocket, or one flagellum was slightly protruding (Fig. 2J). A very well-developed papilla was located anteriorly at the narrowed cell apex and readily observed under a light microscope (Fig. 2J). In old batch cultures, cells diminish their size and a small fraction of these differentiate into a short-lived swimming stage (Fig. 2L), morphologically identical to that of *Natarhynchopus humris* (Tashyreva et al., 2018b). Their cell bodies measured 10.6 to 11.4 μm ($11 \pm 0.3 \mu\text{m}$; $N = 4$) in length and 3.6 to 3.8 μm ($3.7 \pm 0.1 \mu\text{m}$; $N = 4$) in width, while flagella extended 2 to 2.5 times cell body length. Such cells exhibit fast swimming in a straight line, mediated by the anterior flagellum forming a loop, and the posterior one loosely wrapped around the cell body (not shown). During the transition into the swimming stage, the cells become smaller and gradually elongate their flagella (Fig. 2K).

3.3. Fluorescence staining and in situ hybridization

In *R. valaseki*, *R. asiaticus*, and *R. granulatus*, the nucleus lies on the side of the anterior cell half (Figs. 3A, B, C), whereas in *L. aflagellata*, it is located peripherally in the central region (Fig. 3D). Due to the uniform distribution of DNA throughout the mitochondrial lumen, the organelle can be visualized by DAPI staining, which was further confirmed by its co-localization with IFA targeting the mitochondrial ATPase complex (Fig. 3E). The mitochondrion forms a network beneath the cell surface in *R. granulatus* and *R. asiaticus*, whereas in *L. aflagellata* and *R. valaseki*, multiple smaller organelles can be seen at the cell periphery (Figs. 3A, D). Nevertheless, we acknowledge that these might be connected by thin branches lacking DNA and cristae, as was shown for *Lacrimia vacuolata* (Tashyreva et al., 2023).

The screening for bacterial endosymbionts by FISH with Eub338 probe revealed intracellular rod-shaped bacteria in *R. asiaticus* (Fig. 3F).

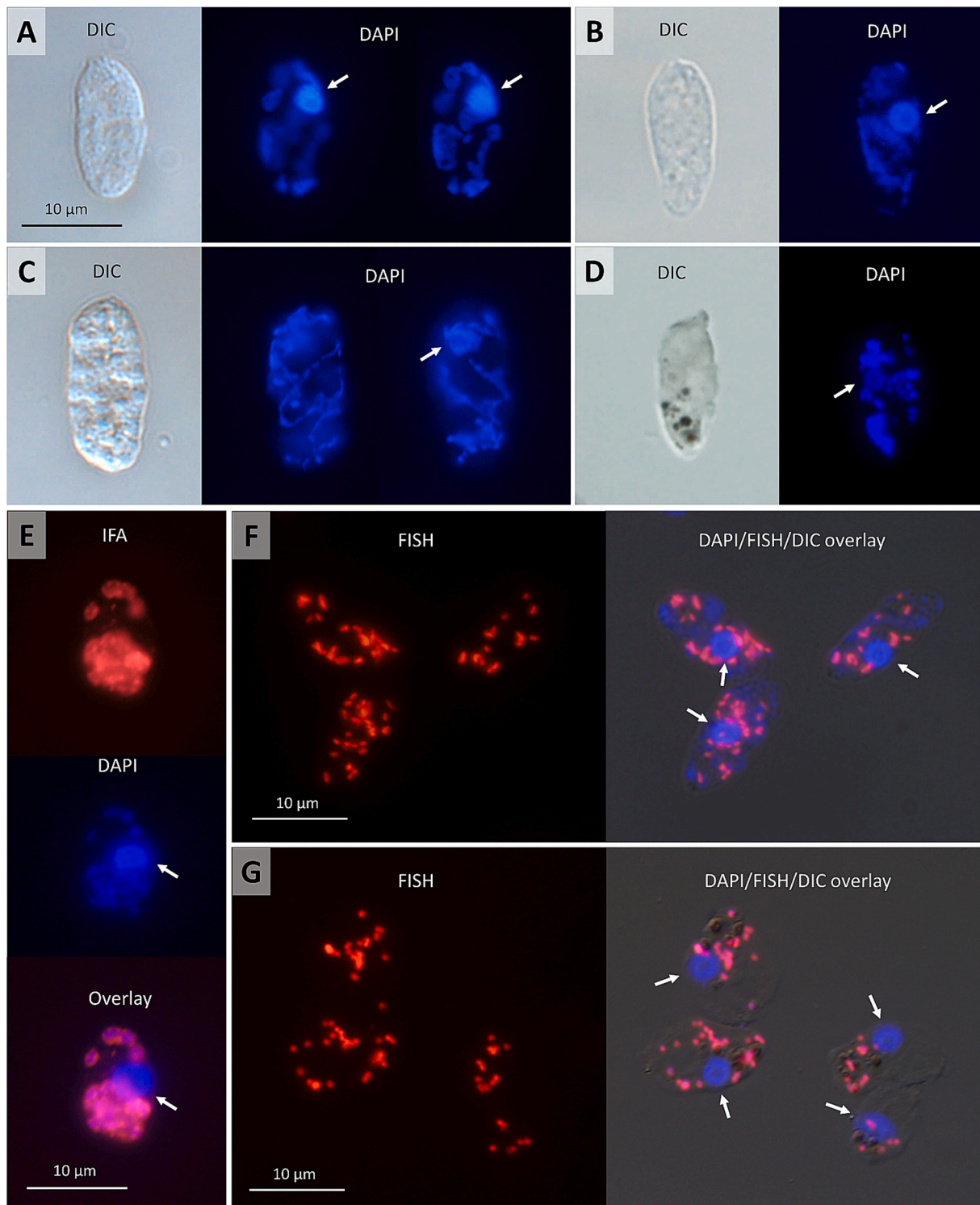


Fig. 3. Differential interference contrast (DIC) and fluorescence microscopy images of chemically-fixed cells. DAPI-stained cells (A–D) of *Rhynchopus valaseki* sp. n. (A), *R. asiaticus* sp. n. (B), *R. granulatus* sp. n. (C), and *Lacrimia aflagellata* sp. n. (D); in A and C, DAPI-staining shows cells in different focal planes. E. Immunofluorescent labeling of mitochondria in *R. valaseki* sp. n. cell with antiserum against ATPase complex. Endosymbiotic bacteria inside *R. asiaticus* sp. n. (F) and *L. aflagellata* sp. n. (G) visualized by hybridization with Eub-338 FISH probe. Arrow points to nucleus.

These were solitary and randomly distributed across the cytoplasm and were not associated with any organelles or subcellular structures. The bacterial load per host cell widely varied between 8 and 37 cells (20.7 ± 5.9 ; $N = 100$); approximately 1 % of *R. asiaticus* cells lacked any endosymbiont. Based on the FISH images, the symbionts measured $\sim 0.9 \mu\text{m}$ in length and $\sim 0.45 \mu\text{m}$ in width. In *L. aflagellata*, intracellular round

bacteria also resided in the cytoplasm, but were either solitary (Fig. 3G) or arranged in clusters. Each *L. aflagellata* cell typically housed 10 to 20 bacteria. See TEM results for a description of the morphology and cell dimensions of the symbionts.

3.4. Phylogenetic analysis of endosymbionts

The 16S rRNA-based maximum likelihood topology confirmed the affiliation of the endosymbiont of *R. asiaticus* to holosporacean genera *Cytopharynx* and *Nesciobacter*, previously described from diplomonads (Tashyreva et al., 2018; George et al., 2020). *Cytopharynx* sp. n. (all symbionts hereafter referred to without the *Candidatus* prefix) branches as a sister taxon to the two *Cytopharynx* species (Fig. 4). Together with *Nesciobacter abundans* from *Diplonema japonicum* and an environmental sequence from a wastewater treatment plant, they form a robustly supported clade branching with *Holosporea*, *Gortzia*, and related environmental sequences nested deeply within the sequenced holosporacean diversity. Given the observed topology and also the sequence similarity to both *Cytopharynx* species (93.7 and 92 %) and *Nesciobacter* (85.7 %) we found the inclusion of these novel endosymbionts into the genus *Cytopharynx* to be well supported.

A partial sequence of the 16S rRNA gene of the *L. aflagellata* endosymbiont (GenBank accession number PP719299) was 99.1 % identical to the already described *Syngnamydia medusae* (Viver et al., 2017). Since no sequences of core proteins used in taxonomy of *Chlamydiae* (Pillonel et al., 2015) are available for this isolate, in accordance with the generally accepted taxonomical rules for bacteria (Kim et al., 2014), we assign this bacterium as an additional isolate of *S. medusae*. Maximum likelihood analysis of the alignment focused on chlamydial symbionts confirms this affiliation. Both *S. medusae* isolates branch together with another isolate from the gills of wrasse *Symphodus melops* (98.7 % and 99.4 % identity), indicating a wide range of putative hosts. The *S. medusae* clade branches with another species of *Syngnamydia* (*S. salmonis* and *S. venezia*) as well as with *Fritschea* sp., *Neptunochlamydia* and several environmental sequences forming a robustly supported clade (Fig. 5). While the current topology makes *Syngnamydia* a paraphyletic taxon, sequence identities within the above described *Syngnamydia* clade (ranging from 93.6 % to 99.1 %) suggest that they all belong to a single genus.

3.5. Cell surface

All species were examined by SEM, which revealed their smooth cell surface lacking extracellular structures. The wrinkled appearance of the plasma membranes is a fixation artifact, which was more pronounced when cells were fixed with paraformaldehyde (Figs. 6D, H, I) compared to OsO₄ (Figs. 6A-C, E-G). The microtubular corset wrapping around the cells can be readily seen beneath the plasma membrane (Figs. 6A, B, E, H). The only exterior structures distinguishable by SEM are the cytostome, the opening to the flagellar pocket (FP), and the papilla associated with them.

All *Rhynchopus* species examined here feature separate openings for the cytostome and the FP (Figs. 6E-G). Among them, only some *R. asiaticus* cells have one flagellum slightly protruding beyond the FP (Fig. 6E). The papilla associated with the cytostome is strictly apical, whereas the FP is situated slightly subapically, giving the cell apex an asymmetric appearance (Fig. 6B). The collar around the cytostome is rounded and thick in *R. valaseki* and *R. asiaticus* (Figs. 6E, F) and slightly thinner in *R. granulatus* (Fig. 6G). It is connected to a small opening to the FP through a long prominent apical papilla (Figs. 6E-G). The cell bodies are cylindrical, with rounded posterior and narrowed anterior ends (Figs. 6A-C).

The *L. aflagellata* cells are dorsoventrally flattened and show notable asymmetry in their apices, introduced by the position and structure of the flagellar and feeding apparatuses, which have a mouth-shaped appearance (Figs. 6D, I). The lower 'lip' is represented by a thick long collar that surrounds the cytostome extending to the FP opening, while the upper 'lip' is formed by a prominent papilla reinforced with dense ridges (Figs. 6D, I). The FP opens 1.5 to 2 µm below the anterior tip. A single, very short flagellum, indistinguishable at the light microscopy level, can be seen projecting outside the FP (Fig. 6I).

3.6. Fine structure

TEM revealed that all four species have generally similar ultrastructure and share most features with other diplomonads. These include a distinct reinforced microtubular band (termed microtubules reinforced or 'MTR') ascending from the bottom of the deep FP (Figs. 7G, 8F, 9H, 10E), looping around the apical cytoplasmic protrusion (papilla) and eventually descending as part of a structurally complex cytopharynx composed of multiple supporting elements (Figs. 7C, 8B, 9C, 10C). The FP and cytopharynxes are positioned at a ~ 30° angle relative to the longitudinal axis (Figs. 7B, F, 8A, H, 9B, I, 10A, B). The flagellar basal bodies are parallel to each other and situated peripherally, close to the plasma membrane (Figs. 7F, 8H, 9I, 10A). The entire cell bodies, except for the FP walls, are subtended by a subplasmalemmal corset of evenly spaced interlinked microtubules that originate from the apical region, helically enclose the entire cell and make a T-junction at the FP level (Figs. 7G, 8F, 9H, 10E). Mitochondrial branches (Figs. 7A, 8A, 9A, 10A) and sacs of endoplasmic reticulum (ER) are peripheral and positioned beneath the microtubular corset (Figs. 7G, M, 8B, 9E, 10G). The nucleus is subspherical, featuring a large nucleolus and electron-dense masses of heterochromatin (Figs. 7A, 8A, 9L, 10K). The Golgi Apparatus (GA) is present as several distinct bodies, each composed of multiple stacked cisternae (Figs. 7G, I, 9C, 10A), usually found in the anterior half of the cell. The cytoplasm is filled with numerous vesicles, inclusions, and vacuoles of various content (see below). All species described here notably lack extrusomes. The discriminating features are provided separately for each species.

3.6.1. *Rhynchopus asiaticus*

The cytopharynx descends more or less parallel to the cell surface before taking a U-turn upwards (Fig. 7B) and eventually makes another turn downwards (not shown). It has a complex structure consistent with that of other *Rhynchopus* species (Nerad, 1990; Roy et al., 2007; Tashyreva et al., 2018b). Its most recognizable features are the ensemble of four elongated petal-shaped ribs attached to the pharyngeal lumen and a peripheral microtubular band (PMB) half-encircling the entire pharyngeal complex (Fig. 7C). A single microtubule contiguous with the MTR band can be seen at the outer tip of each rib (Fig. 7C). The cytopharynx is additionally supported by vertical rods composed of a homogeneous matrix and smaller groups of microtubules (Fig. 7C) and is associated with the ER sacs running along its entire downward length (Fig. 7H). Quadratically-packed bundles of microtubules typical for other diplomonad genera (Tashyreva et al., 2022) are absent from the proximal part of the cytopharynx (not shown). Halfway down its descending part, round, ring-shaped and long endocytic vesicles begin to pinch off the pharyngeal lumen (Figs. 7B, K). The long and ring-shaped vesicles later form concentric double-membrane structures with internalized portions of the cytoplasm (Figs. 7D, E) similar to the digestion-related endomembranous colv organelle of *Lacrimia vacuolata* (Tashyreva et al., 2023). As the cytopharynx descends further, its lumen sharply tapers, while the ribs elongate and become embedded into a dark matrix (not shown but see Fig. 9C for an identical section in *R. granulatus*).

Only the dorsal flagellum slightly projects from the FP. It is notably longer than the ventral flagellum, but it lacks a canonical axoneme. Instead, both flagella stubs contain several solitary microtubules (see Fig. 7G for ventral flagellum) above the distal transitional plate of the flagellum that itself has a conventional structure (Fig. 7G). The FP lining, both flagella, and small vesicles exiting the FP are densely covered with non-tubular hair (Figs. 7F, G). In addition to the MTR, the FP wall is subtended by intermediate and dorsal flagellar roots, composed of six and three microtubules, respectively (Fig. 7G). Furthermore, a group of seven spaced parallel microtubules runs alongside the FP wall (Fig. 7H). The ventral root (not shown) is associated with the outer side of the ventral basal body.

The mitochondrion is generally peripheral (Figs. 7A, B, I), although

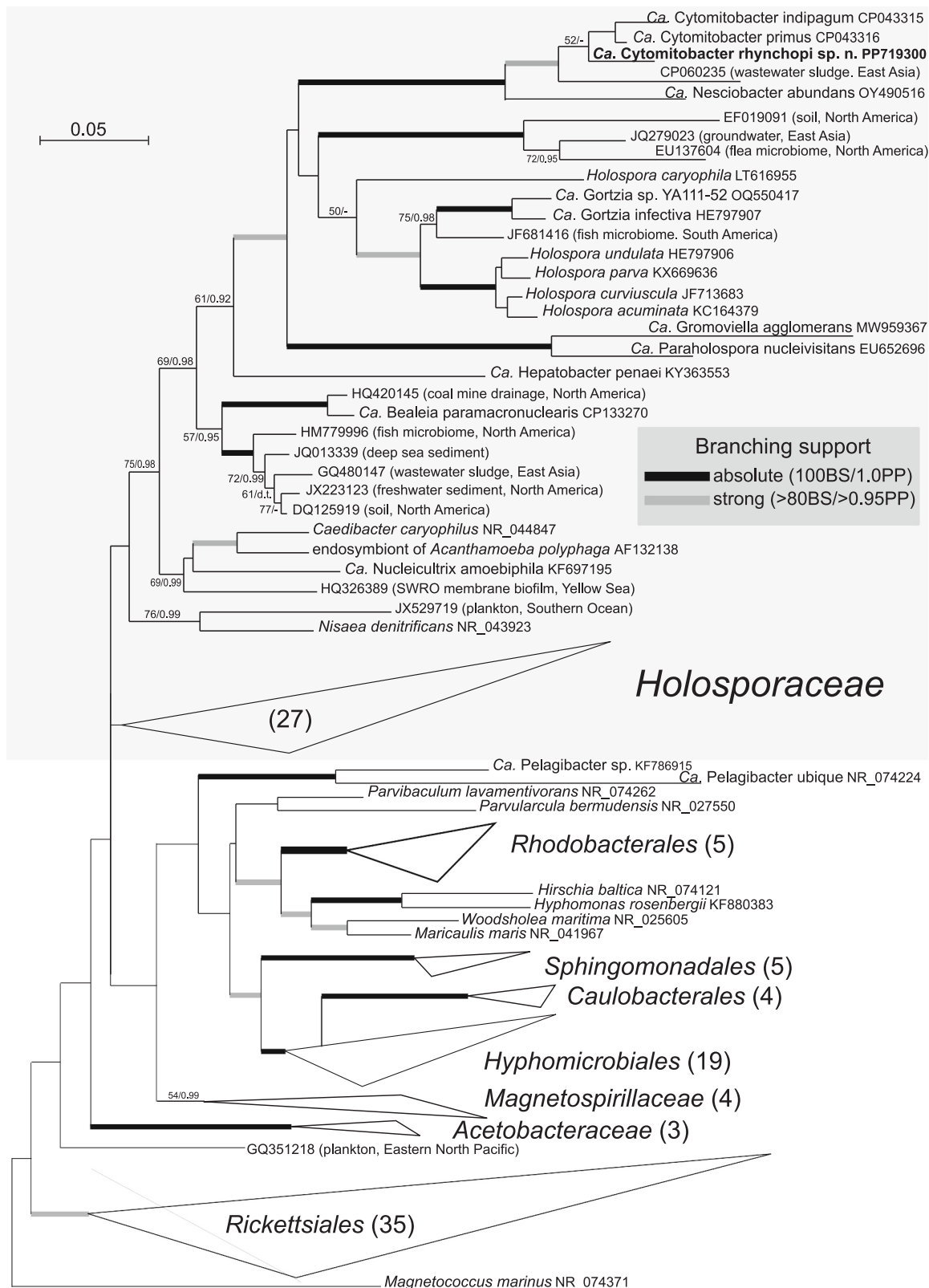


Fig. 4. 16S rDNA maximum likelihood phylogeny showing the position of herein described *Ca. Cytomitobacter rhynchopi* sp. n. The tree is based on the analysis of 145 sequences and 1432 positions under the TVMe+R6 model in IQTree2 (which was selected as the best fitting model using the ModelFinder implemented in IQTree2). The branching support in the form of thickened branches or numbers pointing to relevant nodes represents the non-parametric bootstrap (BS) analysis of 1000 replicates (option -b 1000) using the 'thorough' algorithm in IQTree2 as well as Bayesian posterior probabilities (PP). The latter were estimated from four MCMC chains run in Phylobayes 4.1 under the GTR + C40 model (see Methods for details). Support is shown only for nodes with BS = 80 and higher and/or PP = 0.95 and higher. For readability reasons, some clades that are not directly relevant to the species described are shown as collapsed.

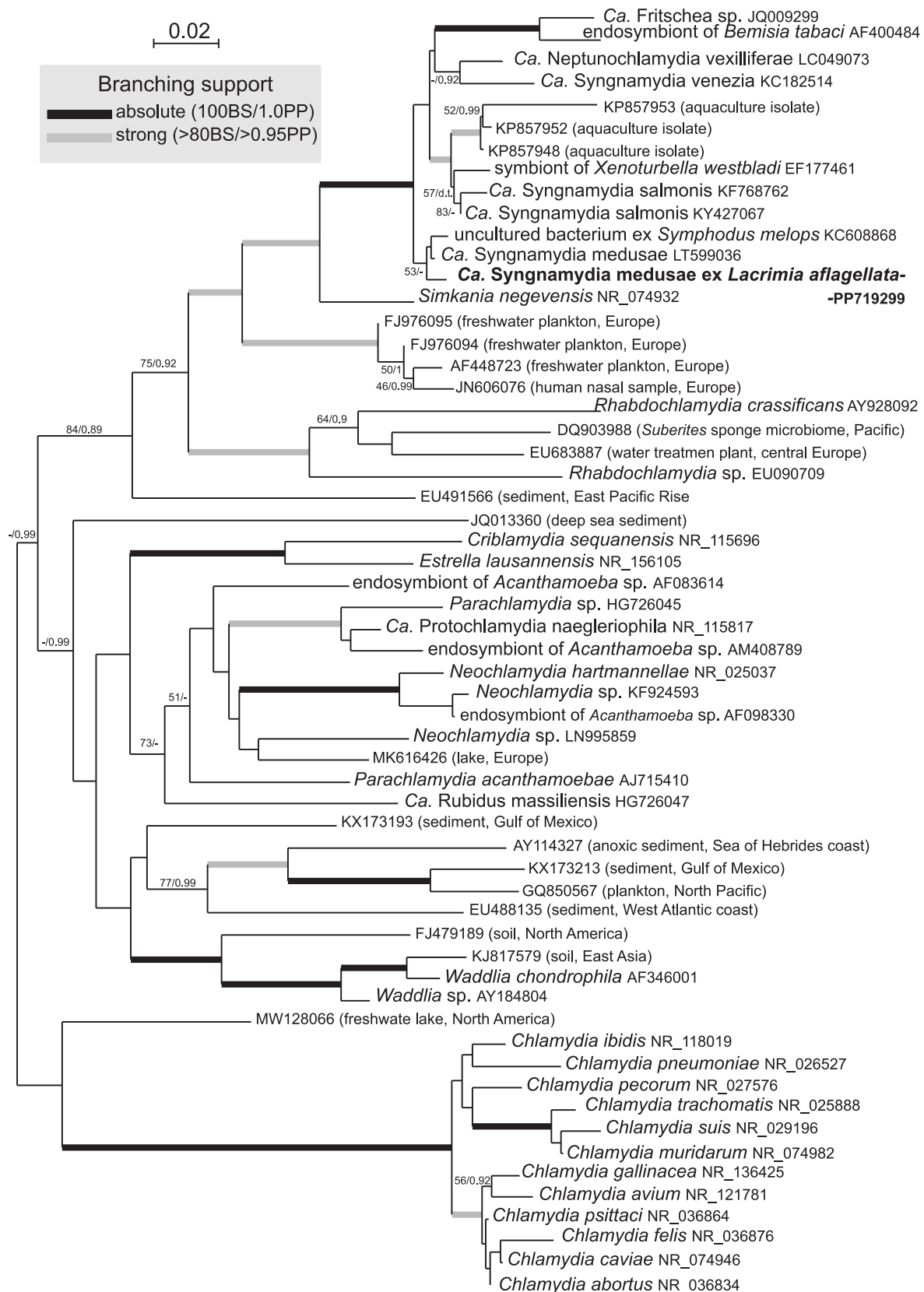


Fig. 5. 16S rDNA maximum likelihood phylogeny showing the affinity of *Ca. Syngnamydia medusae* ex *Lacrimia aflagellata* sp. n. The tree is based on the analysis of 59 sequences and 1510 positions under the GTR + F + I + R4 model in IQTree2 (which was selected as the best fitting model using the ModelFinder implemented in IQTree2). The branching support in the form of thickened branches or numbers pointing to relevant nodes represent the non-parametric bootstrap (BS) analysis of 1000 replicates (option -b 1000) using the 'thorough' algorithm in IQTree2 as well as Bayesian posterior probabilities (PP). The latter were estimated from four MCMC chains run in Phylobayes 4.1 under the GTR + C40 model (see Methods for details). Support is only shown for nodes with BS = 80 and higher and/or PP = 0.95 and higher.

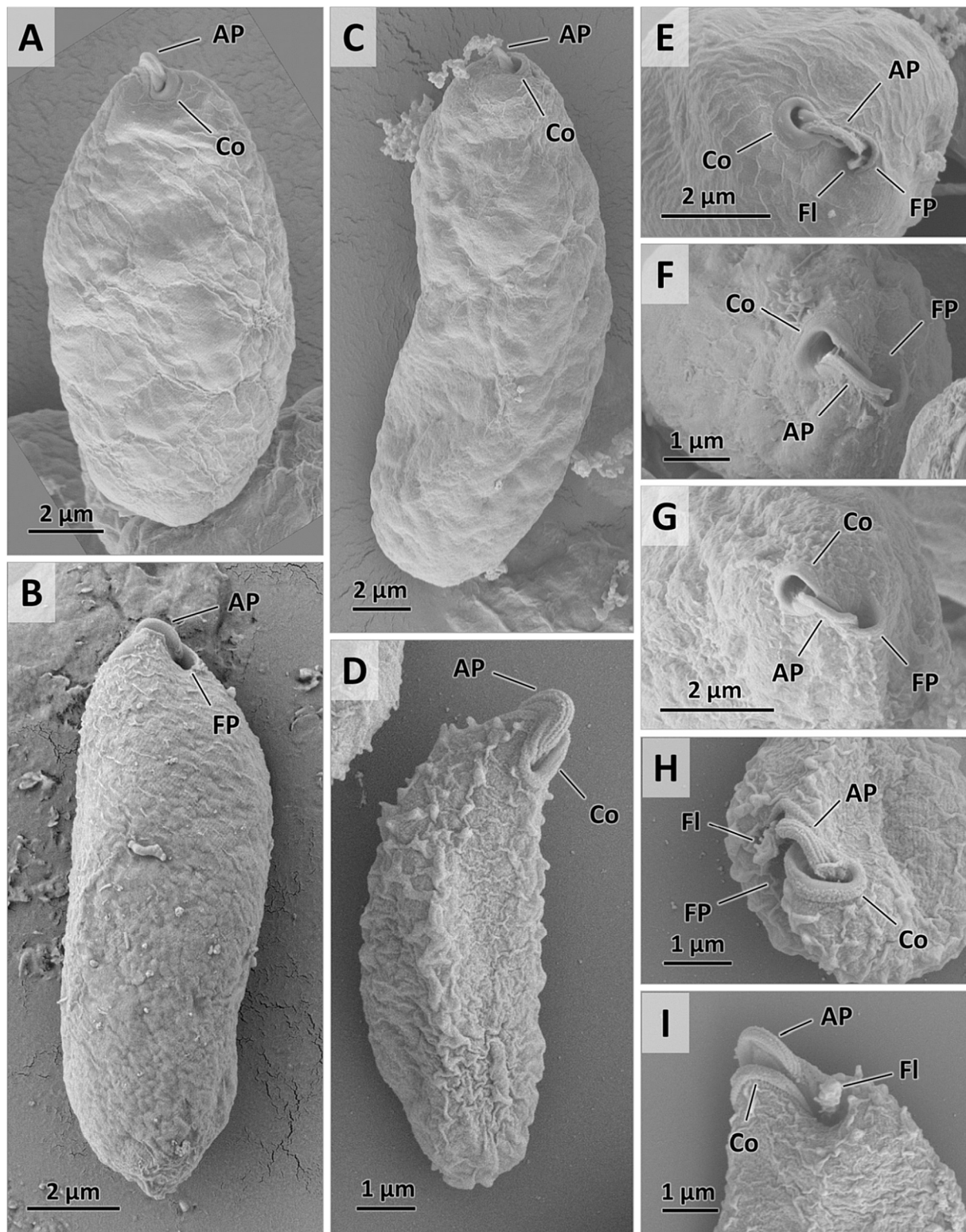
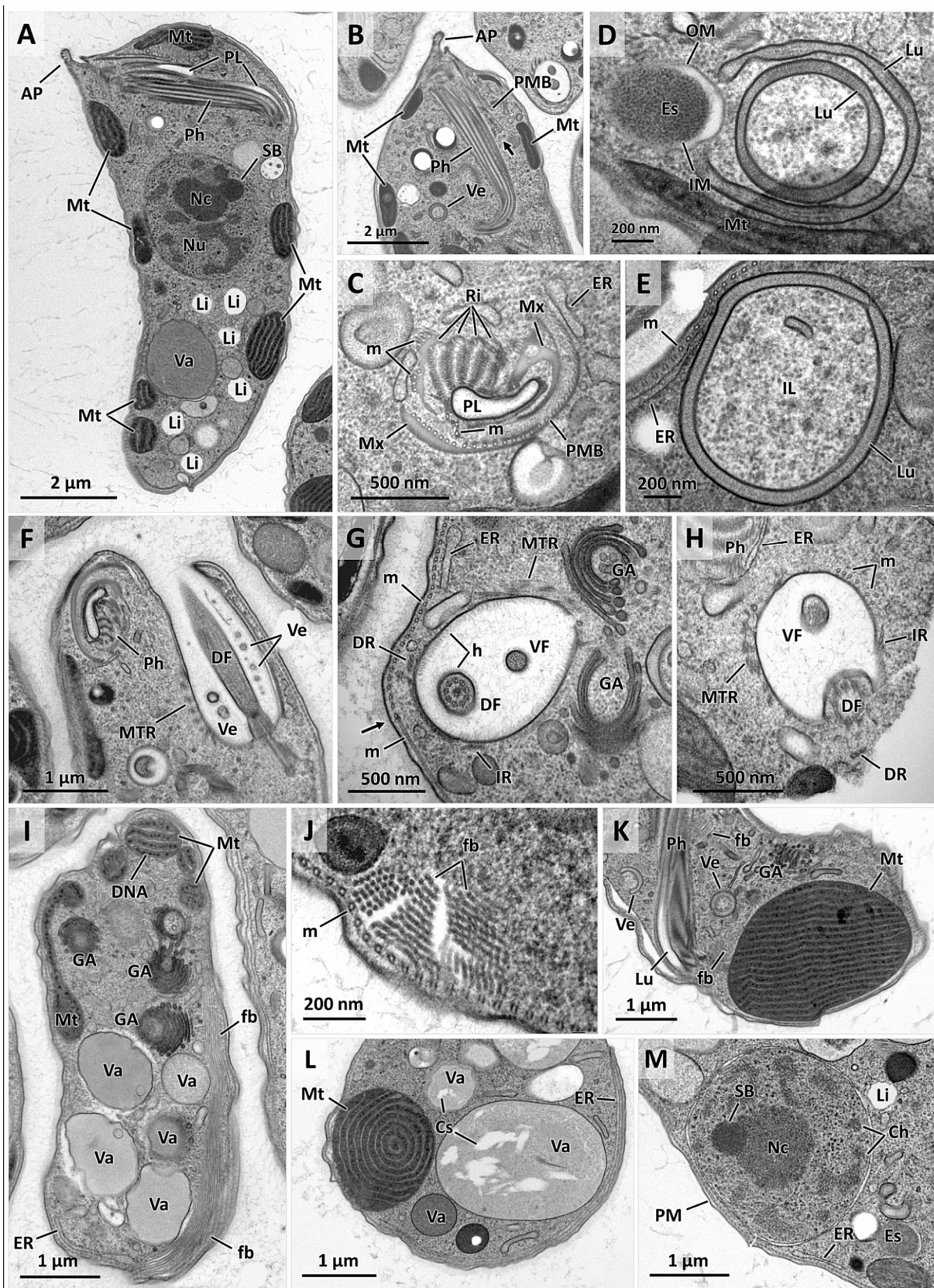


Fig. 6. Scanning electron microscopy images of *Rhynchopus asiaticus* sp. n. (A, E), *Rhynchopus valaseki* sp. n. (B, F), *Rhynchopus granulatus* sp. n. (C, G), and *Lacrimia aflagellata* sp. n. (D, H, I). AP – apical papilla, Co – collar surrounding opening to feeding apparatus, FI – flagellum, FP – entrance to flagellar pocket. Note corset microtubules underneath plasma membrane in A–C, E, and G.

its parts are sometimes seen in the central areas of the cell (not shown). The mitochondrion branches are commonly bulky with numerous prominent and long cristae that form stacks, which usually run parallel to each other and to the cell surface (Figs. 7A, I). Small electron-dense DNA aggregates are evenly interspersed between the cristae (Figs. 7A,

I, K, L). In some cells, exceptionally massive branches of the organelle with parallel or concentric giant cristae were present (Figs. 7K, L). The posterior half of the cell is usually filled with abundant large vacuoles of various texture and opacity, which frequently contain electron-transparent spindle-shaped crystals (Fig. 7L). Small round inclusions



(caption on next page)

Fig. 7. Transmission electron microscopy images of *Rhynchopus asiaticus* sp. n. **A.** Longitudinal section through nucleus and cytopharynx, showing vacuoles and lipid-like inclusions in cell posterior; note that non-apical position of papilla is given by metabolic movement of specimen during sample preparation. **B.** Longitudinal section through apical portion of cell shows typical position of papilla and cytopharynx; note small endocytic vesicles exiting cytopharynx (arrow). **C.** Cross section through distal region of cytopharynx and associated sacs of endoplasmic reticulum. **D.** Cytopharynx-derived long vesicles arranged into structure resembling colv organelle of *Lacrimia vacuolata* and obliquely-sectioned endosymbiont packed with ribosomes and bound by inner and outer plasma membranes. **E.** Colv-like vesicle with enclosed portion of lighter cytoplasm referred to as intraluminal space. **F.** Lengthwise section through dorsal flagellum and flagellar pocket with abundant small vesicles. **G.** Cross-sectioned flagellar roots and flagella; note solitary microtubules in ventral flagellum and T-junction of microtubular corset (arrow). **H.** Cross section through MTR and additional loosely arranged microtubules supporting flagellar pocket wall. **I.** Lengthwise-sectioned posterior half of cell showing several vacuoles, Golgi bodies, and long fiber running along cell periphery. **J.** Cross-sectioned fibers underneath corset microtubules. **K.** Sectioned through massive mitochondrion with numerous flat stacked cristae; note dark DNA aggregates between cristae. **L.** Concentrically-arranged cristae and electron-transparent crystals inside vacuoles. **M.** Nucleus section through nucleolus and spherical body. *AP* – apical papilla, *Ch* – heterochromatin, *Cs* – crystals, *DF* – dorsal flagellum, *DR* – dorsal root, *ER* – endoplasmic reticulum, *Es* – endosymbiont, *fb* – fibers, *GA* – Golgi apparatus, *h* – hairs, *IM* and *OM* – bacterial inner and outer membranes, *IL* – colv intraluminal space, *IR* – intermediate root, *Li* – lipid-like inclusions, *Lu* – colv lumen, *m* – microtubules, *Mt* – mitochondrion, *Mx* – matrix, *Nc* – nucleolus, *Nu* – nucleus, *Ph* – cytopharynx, *PL* – pharyngeal lumen, *PM* – plasma membrane, *PMB* – peripheral microtubular band, *Ri* – ribs, *SB* – spherical body, *Va* – vacuoles, *Ve* – vesicles, *VF* – ventral flagellum.

morphologically identical to lipid droplets in *L. vacuolata* (Tashyreva et al., 2023) can be seen across the cytoplasm (Fig. 7A). The unique feature of *R. asiaticus* is a filament composed of dozens parallel fibers (~17 nm in diameter) that spans across the entire cell, often running along the corset microtubules (Figs. 7I, J, L). The large and subspherical nucleus (up to 2.7 µm) typically appears in the cell periphery, right underneath the corset, and features an electron-dense spherical body adjacent to the prominent nucleolus (Fig. 7M).

The endosymbionts are not localized in proximity to any organelles or cellular structures but rather are randomly distributed within the host cytoplasm. In cross sections, they measure 404 to 576 nm (466 ± 53 nm; $N = 10$) and have typical for α -proteobacteria ultrastructural organization of the cell envelope with a thicker outer and less prominent inner plasma membranes (Fig. 7D). The bacterial cytoplasm is dark and granular due to densely packed ribosomes, lacking any distinguishable intracellular structures.

3.6.2. *Rhynchopus valaseki*

Its cytopharynx is virtually identical to that of *R. asiaticus* in both general architecture and fine structure (Figs. 8A–D). For this species, we additionally illustrate the downward turn of the cytopharynx (Fig. 8D) and its cross-sectioned portion after this turn, which is composed of a semi-circle of microtubules (Fig. 8E). The endocytic vesicles exiting from the cytopharynx are spherical, long, or ring-shaped (Figs. 8C, E, H). They occasionally encircle lipid droplets (Fig. 8C) as in *L. vacuolata* (Tashyreva et al., 2023) and arrange themselves into simple concentric colv-like structures (not shown). The localization and composition of flagellar roots and MTR (Figs. 8F–H) are also identical to the respective structures of *R. asiaticus*, yet a hair coating seems to be greatly reduced or entirely missing from the FP (Figs. 8F–H), while the FP-derived secretory vesicles are small and rare (Fig. 8G). The basal bodies and the flagellar transitional zone, delimited by two cross plates (Fig. 8G), have the conventional arrangement for diplomonids. However, in place of axonemes, flagella above the transitional zone appear as beaded strings in longitudinal sections (Fig. 8H). Neither flagellum has a typical axoneme: in all examined cross sections, only hollow microtubule-free vesicles of variable size were observed (Fig. 8F). Some microtubules were seen in a longitudinally sectioned dorsal flagellum on two occasions (Fig. 8H). Positioned generally in a peripheral manner (Figs. 8A, I, J), the mitochondrial branches often also occupy central parts of cells. The cristae are flat and either parallel or intricately interconnected and interspersed with abundant electron-dense DNA aggregates (Figs. 8I, J). The large peripheral nucleus of *R. valaseki* reaches 2.6 µm in diameter and contains a smaller spherical body embedded in the nucleolus (Fig. 8K). Detailed examination of the TEM sections confirmed the absence of endosymbionts.

3.6.3. *Rhynchopus granulatus*

The architecture of the feeding and flagellar apparatuses (Figs. 9A–I), including associated secretory and endocytic vesicles (Figs. 9F, H), is

identical to those of *R. valaseki*. In Fig. 9D, we additionally demonstrate the proximal region of the cytopharynx before the upward U-turn, which is characterized by the lack of lumen and greatly reduced supporting structures. As in *R. valaseki*, flagella do not bear axonemes above the transitional zone (Figs. 9G–J). Furthermore, although flagella-shaped protrusions can occasionally be seen in longitudinal sections (Fig. 9I), a dedicated search across multiple TEM grids did not reveal any microtubules in transverse sections (Figs. 9G, H, J). The mitochondrial profiles of *R. granulatus* are extensive but typically narrow (Figs. 9A, J), with ample DNA clusters (Figs. 9J, K) and, unlike other *Rhynchopus* species described herein, have extremely sparse short cristae (Fig. 9C). Another distinguishing feature of *R. granulatus* is the copious quantities of large electron-dense inclusions, presumably reserve granules and/or droplets, which are sometimes associated with the mitochondrion (Fig. 9K) or Golgi bodies (not shown). Central and posterior vacuoles with various contents often contain long spindle-shaped crystals (Figs. 9A, K). The nucleus is peripheral, up to 2.7 µm in diameter, and contains a well-defined nuclear body beside the nucleolus (Fig. 9L). Endosymbionts are absent from this species.

3.6.4. *Lacrimia aflagellata*

Although the general architecture of the cytopharynx is similar to the above described *Rhynchopus* species, it is distinguished by lower complexity of its supporting elements, represented by smaller microtubular clusters and fewer and notably thinner vertical rods (Fig. 10C), as well as shorter, less developed ribs that additionally lack an embedding matrix below the tapering point of the pharyngeal lumen (Fig. 10D). The endocytic vesicles form elaborated reticulated structures (Figs. 10B, D) similar to the colv organelle of *L. vacuolata* (Tashyreva et al., 2023). Both dorsal and intermediate roots ascend along the FP wall, but the latter is positioned more proximally and has a 6 + 1 configuration (Fig. 10E). In the trophic stage, the flagella are short and nearly fully concealed inside the FP, yet, unlike all *Rhynchopus* species, they bear a typical eukaryotic axoneme (Fig. 10E) without a paraflagellar rod (PFR). Interestingly, the dorsal flagellum is always longer than the ventral one and sometimes appears to have one or two additional microtubules between the central pair and outer doublets (Fig. 10G). The entire cell apex, including the cytostome, papilla, flagella, FP walls and secretory vesicles, are densely covered with hairs (Fig. 10G). The basal bodies, interconnected by a fiber, and transitional zones of axonemes are of conventional for diplomonids structure (Figs. 10A, H). In the swimming stage, the flagella become thickened with lattice-like PFR (Fig. 10F). The mitochondria are strictly peripheral, with alternating vesicular and long or short flat cristae (Fig. 10I), morphologically similar to the cristae of *L. vacuolata* (Tashyreva et al., 2023). A smaller nucleus (up to 1.8 µm in diameter) is distinguished by a prominent granular nucleolus surrounded by dark masses of heterochromatin (Fig. 10K) and the lack of a spherical body. Bacterial endosymbionts, either solitary or in clusters of variable size, are pleomorphic (Fig. 10A) with at least two distinguishable morphotypes. A larger spherical type with lighter homogenous granular

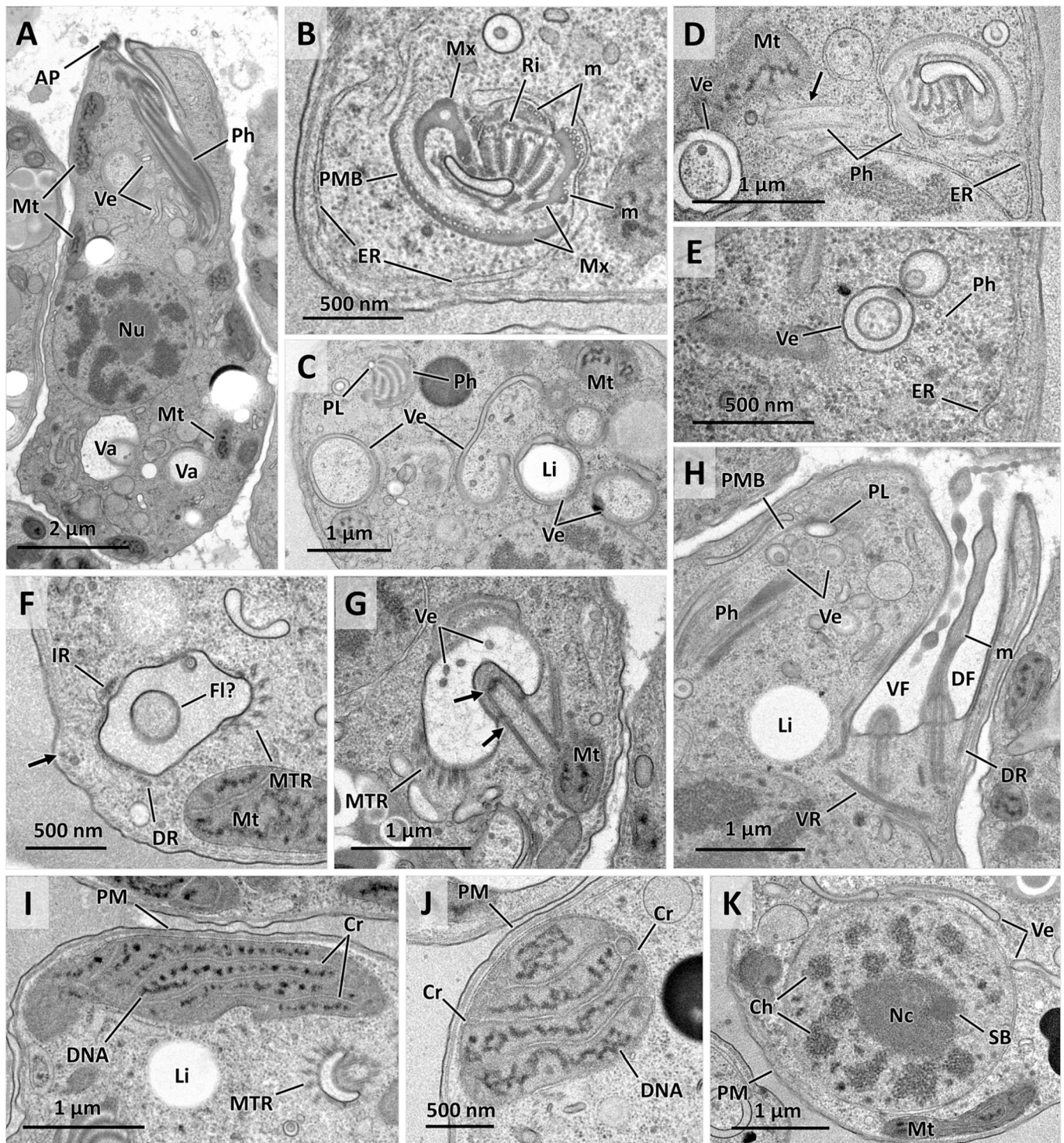


Fig. 8. Transmission electron microscopy images of *Rhynchopus valaseki* sp. n. **A.** Longitudinal section through nucleus, cytopharynx, and posterior vacuoles. **B.** Cross-sectioned distal part of cytopharynx with associated endoplasmic reticulum. **C.** Cytopharynx-derived vesicles surrounding portions of cytoplasm and lipid-like inclusions. **D.** Cross section through distal part of cytopharynx and its lengthwise-sectioned downward turn. **E.** Semi-circle of pharyngeal microtubules after downward turn and cytopharynx-derived vesicles. **F.** Cross-section through flagellar pocket showing dorsal and intermediate roots and T-junction of microtubular corset (arrow); note lack of microtubules inside 'flagellum'. **G.** Longitudinal section through flagellum; arrows point at proximal and distal plates delimiting transition zone of flagellum. **H.** flagella in longitudinal section and cytopharynx in oblique section; note small vesicles exiting cytopharynx. **I.** Mitochondrial branch with stacked nearly parallel cristae and dark DNA inclusions. **J.** Mitochondrial branch with stacked and interconnected cristae. **K.** Nucleus sectioned through nucleolus and spherical body. AP – apical papilla, Ch – heterochromatin, Cr – cristae; DF – dorsal flagellum, DR – dorsal root, ER – endoplasmic reticulum, FI – flagellum, IR – intermediate root, Li – lipid-like inclusions, m – microtubules, Mt – mitochondrion, Mx – matrix, Nc – nucleolus, Nu – nucleus, Ph – cytopharynx, PL – pharyngeal lumen, PM – plasma membrane, PMB – peripheral microtubular band, Ri – ribs, SB – spherical body, Va – vacuoles, Ve – vesicles, VF – ventral flagellum, VR – ventral root.

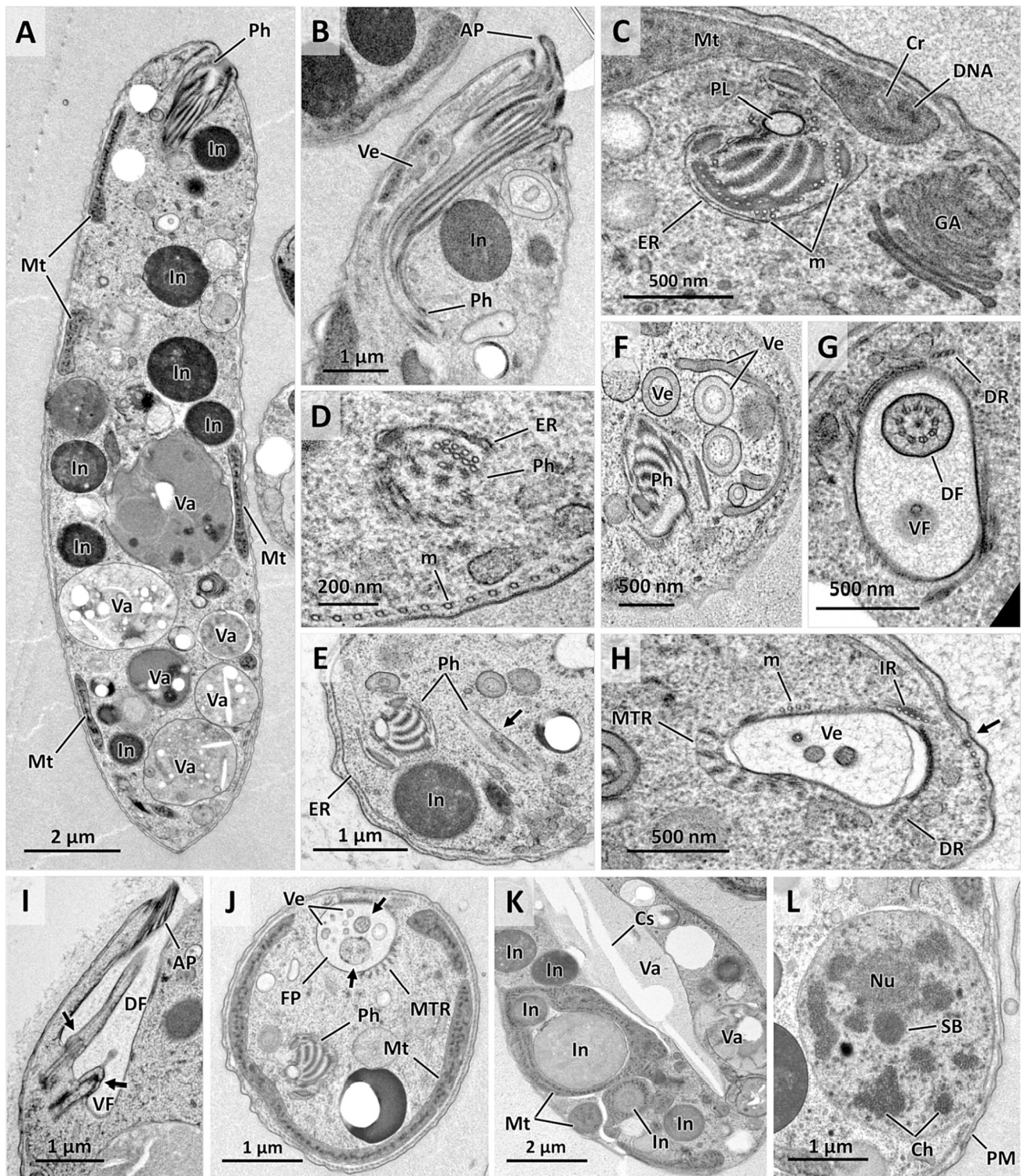


Fig. 9. Transmission electron microscopy images of *Rhynchopus granulatus* sp. n. **A.** Longitudinal section through entire cell displays numerous inclusions and vacuoles. **B.** Lengthwise-sectioned cytopharynx; note small endocytic vesicles exiting it. **C.** Cross-sectioned proximal part of cytopharynx, half-encircled with endoplasmic reticulum. **D.** Cross-sectioned cytopharynx at its upward U-turn; note lack of most supporting elements. **E.** Downward turn of cytopharynx marked with *arrow* and corset microtubules. **F.** Cytopharynx-derived tubular and ring-shaped vesicles. **G.** Cross section through transitional zone of dorsal flagellum and tip of ventral flagellum. **H.** Cross-sectioned flagellar pocket showing dorsal and intermediate roots, MTR, four additional microtubules, and microvesicles; *arrow* points to T-junction of corset microtubules. **I.** Flagella in longitudinal section; *arrows* point to distal plates. **J.** Cross section through anterior half of cell with mitochondrion occupying most of cell periphery; note vesicles and 'flagella' lacking microtubules (*arrows*). **K.** Inclusions associated with mitochondrion and long crystal inside vacuole. **L.** Nucleus sectioned through nucleolus and spherical body. AP – apical papilla, Ch – heterochromatin, Cr – cristae, DF – dorsal flagellum, DR – dorsal root, ER – endoplasmic reticulum, GA – Golgi apparatus, In – inclusions; IR – intermediate root, m – microtubules, Mt – mitochondrion, Mx – matrix, Nc – nucleolus, Nu – nucleus, Ph – cytopharynx, PL – pharyngeal lumen, PM – plasma membrane, Ri – ribs, SB – spherical body, Va – vacuoles, Ve – vesicles, VF – ventral flagellum.

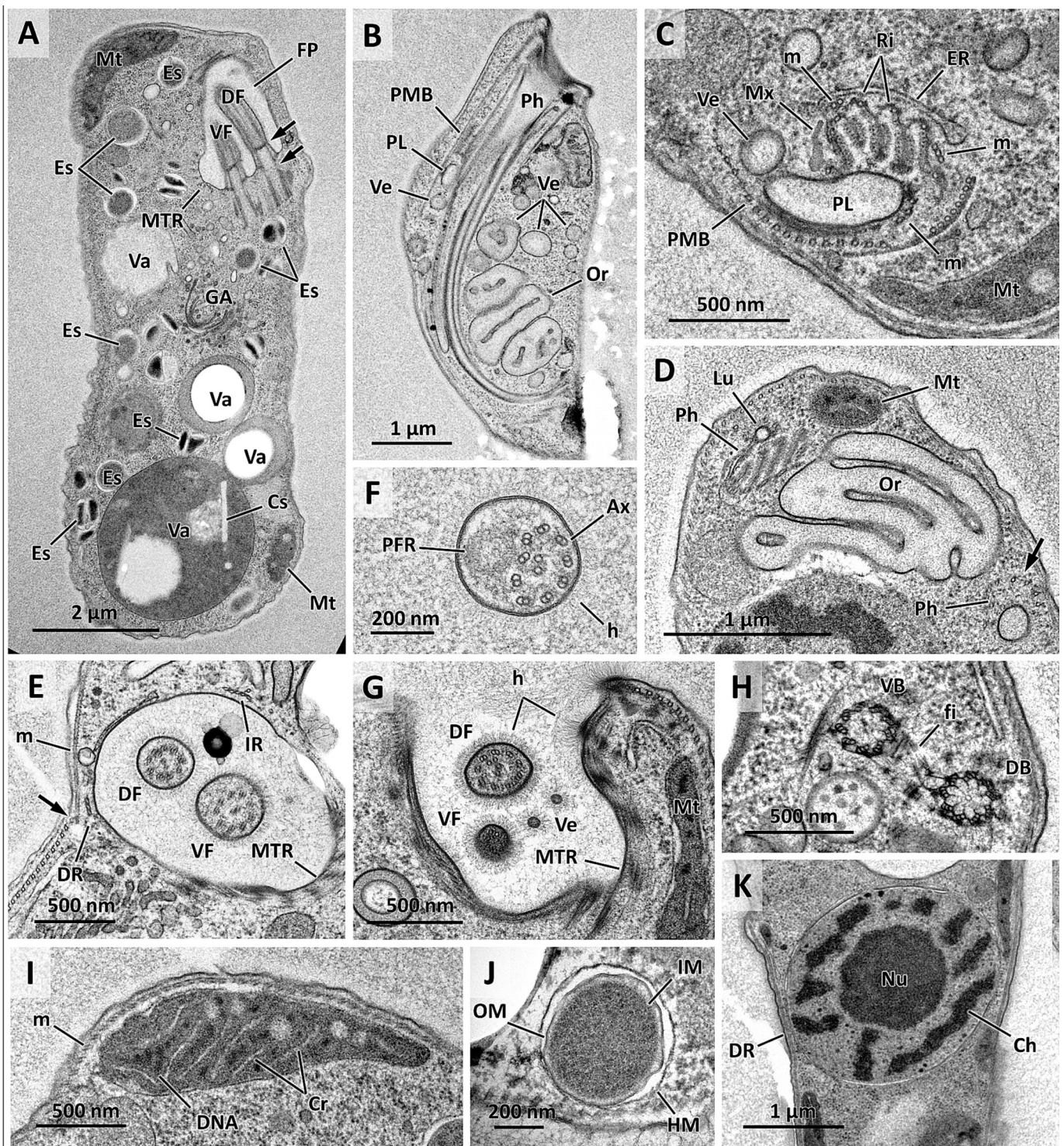


Fig. 10. Transmission electron microscopy images of *Lacrimia aflagellata* sp. n. **A.** Tangential-longitudinal section of cell through flagellar pocket; *arrows* point to transitional plates of lengthwise-oriented flagella; note numerous endosymbionts scattered across cytoplasm. **B.** Longitudinal cytopharyngeal profile with emerging endocytic vesicles and colv-like organelle. **C.** Transverse cytopharyngeal profile sectioned through middle of downward turn. **D.** Close view of colv-like organelle; *arrow* points to upward turn of cytopharynx. **E.** Cross section through flagella and flagellar roots; microtubular corset T-junction is marked with *arrow*. **F.** Dorsal flagellum of swimming stage with circular cross-sectioned paraflagellar rod and hair coating. **G.** View of flagellar pocket beneath its opening shows dense hair coating of flagella, cell apex, and small vesicles; note two additional microtubules in dorsal flagellum. **H.** Dorsal and ventral basal bodies of flagellum connected via fiber. **I.** Mitochondrion with flat short and vesicular cristae. **J.** Close view of symbiont bound by inner and outer bacterial membrane and additional host membrane. **K.** Peripheral nucleus sectioned through nucleolus and heterochromatin. *AP* – apical papilla, *Ax* – axoneme, *Ch* – heterochromatin, *Cs* – crystals, *DF* – dorsal flagellum, *DR* – dorsal root, *ER* – endoplasmic reticulum, *Es* – endosymbiont, *fb* – fibers, *GA* – Golgi apparatus, *h* – hairs, *HM* – host membrane, *IM* and *OM* – bacterial inner and outer membranes, *IR* – intermediate root, *m* – microtubules, *Mt* – mitochondrion, *Mx* – matrix, *Nc* – nucleolus, *Nu* – nucleus, *Or* – colv organelle, *pH* – cytopharynx, *PL* – pharyngeal lumen, *PM* – plasma membrane, *PMB* – peripheral microtubular band, *Ri* – ribs, *Va* – vacuoles, *Ve* – vesicles, *VF* – ventral flagellum.

cytoplasm is consistent with a chlamydial reticulate body, while a smaller lens, polygonal, or irregularly shaped type with a very dark interior is referred to as an elementary body (Israelsson, 2007). Both types are bound by the inner and outer bacterial membranes and an additional host-derived membrane (Fig. 10J). The reticulate body morphotype is 418 to 498 nm in diameter (454 ± 23 nm; $N = 12$).

4. Discussion

Although considered obsolete by some biologists, detailed morphological descriptions have not lost their informative power and remain indispensable for establishing proper taxonomic placement, as well as for our understanding the ecology as well as molecular and cell biology of a given organism. Among all eukaryotes, this is probably most true for protists, and especially for heterotrophic flagellates. Here we provide a detailed morphological description of four new marine diplomonids, accompanied by their 18S rRNA genes, as well as the 16S rRNA genes of their endosymbiotic bacteria.

In the new species, we have found all ultrastructural features previously observed in diplomonids (Nerad, 1990; Montegut-Felkner and Triemer, 1996; Simpson, 1997; Tashyreva et al., 2022). While there is no data for Eupelagonemidae and the DSPD II clade, the representatives of Diplonemidae and Hemistasiidae show considerable ultrastructural similarity. This applies to the cell surface, microtubular cytoskeleton, nucleus, peripheral position and reticulated nature of their mitochondrion, endomembrane system, and overall structure of the feeding and flagellar apparatuses (Tashyreva et al., 2022, 2023), although the composition of the latter two is subject to slight variations. Feeding apparatuses among diplomonids differ mainly by the prominence of their cytostomal C-shaped collars, the size of the apical papilla, and the complexity of the cytopharynx, which varies by the thickness of the supporting rods, the amount of embedding matrix, the length of the ribs, and the presence of additional bundles of microtubules in its proximal part. Flagellar apparatuses are distinguished by the composition of axonemes and the position of the flagellar pocket relative to the cell apical tip (Nerad, 1990; Simpson, 1997; Tashyreva et al., 2022, 2023). Finally, the abundance, branching, shape, and length of mitochondrial cristae are subject to species-specific variation. The most common arrangement is abundant long flat cristae in stacked configuration, although short, non-parallel, branched, and very sparse cristae are also encountered (Tashyreva et al., 2022), often being strikingly different in closely related *Rhynchopus* species described herein.

Since its initial discovery (Skuja, 1948), the genus *Rhynchopus* has been characterized by a large gliding trophic stage with short flagellar stubs concealed inside the flagellar pocket, which in nearly all species differentiates into a smaller fast-swimming stage with long flagella thickened by a PFR (Nerad, 1990; Schnepf, 1994; Simpson, 1997; von der Heyden et al., 2004; Roy et al., 2007; Tashyreva et al., 2018b). Although the molecular divergence of their 18S rRNA gene in some cases was considerable (>15 %), all new species fitting this description were assigned to the genus *Rhynchopus* (Tashyreva et al., 2018b). However, since this combination of characters is no longer unique to *Rhynchopus* in the original concept due to the discovery of another, phylogenetically rather distantly related *L. aflagellata* described here, a taxonomic revision of the genus *Rhynchopus* is timely. Apart from the divergence of 18S rRNA gene (83.5 to 88.3 % identity to *Rhynchopus* spp. sequences) and their robustly supported sister position to *Rhynchopus* spp. (Fig. 1), representatives of *Natarhynchopus* gen. n. are distinguished by a significantly smaller size (mean length is 14.5 μ m compared to ~16–27 μ m in *Rhynchopus* spp.), notably increased agility (observed as fast gliding and frequent metabolic movements), and frequent differentiation into the swimming stage following starvation, in contrast to rare or absent differentiation in *Rhynchopus* spp. Since the of 18S rRNA gene similarity within the genus *Rhynchopus* (as defined here) ranges from 85 to 96.2 % identity between its representatives (Supplementary Table 1), further separation into several genera is possible with increased sampling.

Previously, the ability to convert to the swimming stage has been documented in all starved *Rhynchopus* species, albeit often at low frequency (Nerad, 1990; Simpson, 1997; Roy et al., 2007; Tashyreva et al., 2018b), whereas this trait has not been investigated in *R. amitus* and *R. coscinodiscivorus* (Skuja, 1948; Schnepf, 1994). Here, we describe three *Rhynchopus* species that do not produce any such cells following starvation. However, we acknowledge that the environmental cues triggering such differentiation may be more complex than simply the lack of nutrients in the medium. This is the case for *Diplonema aggregatum*, which requires the addition of small amounts of nutrient agar following the initial starvation in order for swimming cells to emerge (Tashyreva et al., 2018a). Furthermore, while *R. asiaticus* maintains slow gliding motility typical of this genus and preserves solitary microtubules in its flagellar stubs, *R. valaseki* and *R. granulatus* appear to lack these characters, at least under laboratory conditions. At the same time, the general morphology (size and shape, flagella concealed within the FP), motility (fast gliding on surfaces), and life stage history (trophic stage gradually transitioning to the swimming stage with flagella thickened by the PFR) of *L. aflagellata* closely resemble those of *Natarhynchopus humris* (Tashyreva et al., 2018b). The only important distinction is the presence of a conventional axoneme inside flagellar stubs of *L. aflagellata* rather than the solitary microtubules of *Rhynchopus* spp. (Tashyreva et al., 2022). Although *L. aflagellata* does not have the teardrop-shaped bodies, large posterior vacuoles, and permanently long flagella typical for *Lacrimia* spp., it carries a number of ultrastructural traits characteristic for the genus. These include the complex architecture of the mitochondrial cristae, the reduced thickness of the dense matrix associated with the cytopharynx, and the colv organelle (Tashyreva et al., 2018b, 2023). The latter seems to be present also in the *Rhynchopus* species described herein, albeit in a highly simplified form (see Figs. 7D, E).

In conclusion, only a few morphological, ultrastructural, motility, and life cycle traits can serve as unique apomorphies for specific clades, as the major discriminating features tend to be scattered throughout the diplomonid tree (Nerad, 1990; Tashyreva et al., 2018a, 2022). This is further supported by the description of *L. aflagellata*, which closely resembles *Rhynchopus/Natarhynchopus* species in terms of morphology, motility, and life cycle history (this work). Currently, only a prominent colv organelle appears to be specific to the genus *Lacrimia* (this work), while the presence of peripheral lacunae unifies members of Hemistasiidae (Tashyreva et al., 2022).

In this study, we identified chlamydial and holosporacean endosymbionts in two new diplomonid species. *Holosporaceae* is a family of obligate intracellular bacteria dwelling almost exclusively within protist hosts such as ciliates and amoebozoans (Muñoz-Gómez et al., 2019; Giovannini et al., 2024). Together with three other species, namely *C. primus*, *C. indipagum*, and *Nesciobacter abundans*, the new representative *C. rhynchopi* forms a robustly supported clade, whose members are restricted to diplomonids (George et al., 2020). Another sequence branching within the clade (GenBank accession number CP060235; Fig. 4) is derived from a metagenome-assembled genome of an activated sludge bacterium (Liu et al., 2021). Given the freshwater lifestyle of some diplomonids (Kostygov et al., 2021; Mukherjee et al., 2019), it is entirely plausible that the organism hosting this bacterium is a diplomonid. Unlike three other members of *Holosporaceae* found within diplomonids (Tashyreva et al., 2018a; George et al., 2020), *C. rhynchopi* is randomly distributed throughout the cytoplasm of *R. asiaticus* and shows no evidence of interaction with the mitochondrion or other cellular structures. Unlike other holosporaceans (Görtz and Schmidt, 2015), those found in diplomonids are unable to differentiate into morphologically distinct infectious forms, at least under cultivation conditions.

In contrast to the holosporacean symbionts, *Chlamydiae* associated with diplomonids are capable of infecting a wide range of hosts. In the case of *Syngnamydia medusae*, three very closely related organisms, sharing >98.65 % identity of their 16S rRNA gene sequences, were found inside a ciliate from the digestive cavity of a jellyfish (Viver et al.,

2017), epithelial cells of a wrasse fish (GenBank accession number KC608868), and finally, in a diplomonid *L. aflagellata* (this work). Based on their high 16S rRNA similarity and according to the cut-off values established to distinguish bacterial taxa (Kim et al., 2014), these bacteria likely belong to the same species, although the gene in question may lack taxonomic resolution at the species level (Pillonel et al., 2015). Following the same cut-off value (98.65 %), another chlamydial symbiont, *Syngnamydia salmonis*, was described from the epithelial cells of Atlantic salmon *Salmo salar* (Nylund et al., 2015), an amoebozoan *Paramoeba perurans* (Nylund et al., 2018), and a diplomonid *Rhynchopus euleeides* (GeneBank accession number OY735137) (our unpublished data).

These findings suggest that diplomonids may serve as vectors mediating the transmission of chlamydial pathogens in fish populations. This notion is further supported by the lifestyle of many diplomonids, which includes *endo*- and *ectoparasitism* on multicellular marine organisms (Bodammer and Sawyer, 1981; Kent et al., 1987; von der Heyden et al., 2004; Tashyreva et al., 2022). Both *L. aflagellata* and *R. euleeides* differentiate into a highly motile swimming stage (Roy et al., 2007; this work), which is thought to be involved in the dissemination and infection of multicellular organisms. In this case, chlamydial symbionts may benefit their diplomonid host by causing lysis of the fish epithelium, thus providing this soft naked flagellate with a means of entry into a host.

4.1. Taxonomic Summary based on ICZN

Phylum Euglenozoa Cavalier-Smith, 1981.
Class Diplonemea Cavalier-Smith, 1993.
Family Diplonemidae Cavalier-Smith, 1993.
Genus *Rhynchopus* Skuja, 1948.

4.1.1. *Rhynchopus asiaticus* Tashyreva, Horák et Lukeš, sp. n

Species designated based on the discrepancy in 18S rRNA gene with *Rhynchopus* spp. (less than 96 % identity).

Description: colorless naked biflagellate; only trophic stage detected; cylindrical cell bodies with rounded posterior and slightly narrowed anterior, 12.4 to 23.6 µm long (15.9 ± 2.5 µm; $N = 51$) and 3.9 to 5.9 µm wide (5.3 ± 0.6 µm; $N = 51$); flagella with solitary microtubules in axonemes, lacking paraflagellar rods; ventral flagellar stub concealed inside flagellar pocket, dorsal slightly protruding beyond flagellar pocket; metabolic; move by slow gliding on surfaces; well-developed collar around cytostome; narrow papilla; characteristic filament composed of dozens parallel fibers (~17 nm in diameter) spanning across entire cell; long flat mitochondrial cristae arranged in stacks; mitochondrion not strictly peripheral; spherical perinucleolar body; extrusomes absent; intracellular bacterial symbiont *Ca. Cytomitobacter rhynchopi*.

Etymology: *asiaticus*, refers to the Asian origin of the species; adjective.

Type strain: *Rhynchopus asiaticus* YZ270 clone10.

Type material: hapantotype is a block of resin-embedded cells for transmission electron microscopy deposited in the protozoological collection of the Institute of Parasitology, Biology Centre, Czech Academy of Sciences, České Budějovice, Czech Republic under no. IPCAS Pro 85.

Gene sequence: NCBI acc. n. PP719296.

Type locality: water collected at 270 m depth at the Shizuoka prefectural deep-sea water pumping facility, Yaizu, Japan.

ZooBank: DBB0197A-205C-432C-9E23-A85A55795064.

4.1.2. *Rhynchopus valaseki* Tashyreva, Horák et Lukeš, sp. n

Species designated based on the discrepancy in 18S rRNA gene with *Rhynchopus* spp. (less than 96 % identity).

Description: colorless naked biflagellate; only trophic stage detected; variable in size cylindrical cell bodies with rounded posterior and slightly narrowed anterior, measuring from 7.9 to 19.9 µm in length

(12.9 ± 2.9 µm; $N = 54$) and 3.0 to 7.6 µm in width (5.2 ± 0.9 µm; $N = 54$); flagellar stubs appearing as ‘beaded strings’ concealed inside flagellar pocket, axonemal microtubules occasionally present only in dorsal flagellum, lacking paraflagellar rods; metabolic only when immobilized between slides; no gliding; well-developed collar around cytostome; narrow papilla; flat branched mitochondrial cristae; mitochondrion not strictly peripheral; spherical perinucleolar body; extrusomes absent; endosymbionts absent.

Etymology: *valaseki*, named after Leoš Shivaya Valášek, who significantly contributed to our understanding of translation in protists.

Type strain: *Rhynchopus valaseki* YZ270 clone 9.

Type material: hapantotype is a block of resin-embedded cells for transmission electron microscopy deposited in the protozoological collection of the Institute of Parasitology, Biology Centre, Czech Academy of Sciences, České Budějovice, Czech Republic under no. IPCAS Pro 87.

Gene sequence: NCBI acc. n. PP719297.

Type locality: water collected at 270 m depth at the Shizuoka prefectural deep-sea water pumping facility, Yaizu, Japan.

ZooBank: 794A7D8E-E523-4C9E-9F57-71FEF9FCF8A2.

4.1.3. *Rhynchopus granulatus* Tashyreva, Horák et Lukeš, sp. n

Species designated based on the discrepancy in 18S rRNA gene with *Rhynchopus* spp. (less than 96 % identity).

Description: colorless naked biflagellate; only trophic stage detected; cylindrical cell bodies with rounded posterior and constricted anterior, 16.3 to 28.2 µm in length (21.6 ± 6.8 µm; $N = 69$) and 4.8 to 8.7 µm in width (6.8 ± 0.8 µm; $N = 69$); heavy cytoplasmic granulation; flagellar stubs appearing as ‘beaded strings’ concealed inside flagellar pocket; axonemal microtubules and paraflagellar rods absent; metabolic only when immobilized between slides; no gliding; well-developed collar around cytostome; narrow papilla; mitochondrion not strictly peripheral; very sparse short and flat mitochondrial cristae; spherical perinucleolar body; common long needle-shaped crystals inside central vacuoles; extrusomes absent; endosymbionts absent.

Etymology: *granulatus*, denotes dense cytoplasmic granulation; adjective.

Type strain: *Rhynchopus granulatus* DT0508.

Type material: hapantotype is a block of resin-embedded cells for transmission electron microscopy deposited in the protozoological collection of the Institute of Parasitology, Biology Centre, Czech Academy of Sciences, České Budějovice, Czech Republic under no. IPCAS Pro 86.

Gene sequence: NCBI acc. n. PP719298.

Type locality: seawater spider crab tank at the Enoshima aquarium, Fujisawa, Japan.

ZooBank: BBF9C9C1-0415-4C4D-B068-E6E6AAD3677E.

Phylum Euglenozoa Cavalier-Smith, 1981.

Class Diplonemea Cavalier-Smith, 1993.

Family Diplonemidae Cavalier-Smith, 1993.

Genus *Lacrimia* Tashyreva, Prokopcuk, Horák et Lukeš, 2018.

4.1.4. *Lacrimia aflagellata* Tashyreva, Horák et Lukeš, sp. n

Species designated based on the discrepancy with *L. lanifica* and *L. vacuolata* in 18S rRNA gene (less than 92.5 % identity) and morphology. Distinguished from other *Lacrimia* species by the presence of the trophic and swimming stages, gliding motility in the trophic stage, prominent papilla, as well as smaller size and the lack of teardrop-shaped morphology of their bodies.

Description: colorless naked biflagellate; long well-developed collar around cytostome extending to flagellar pocket opening; prominent papilla with pronounced ridges; large opening to flagellar pocket; highly metabolic; peripheral mitochondrion with flat and vesicular cristae; spherical perinucleolar body not detected; lack of large posterior vacuoles; intracellular bacterial symbiont *Ca. Syngnamydia medusae*.

In trophic stage: flattened cell bodies with rounded posterior and

bent anterior end, 10.2 to 16.7 μm ($14.1 \pm 1.5 \mu\text{m}$; $N = 60$) long, 4.1 to 5.6 μm ($4.7 \pm 0.4 \mu\text{m}$; $N = 60$) wide; flagellar stubs bearing conventional axonemes, often with one or two additional microtubules in dorsal flagellum, without paraflagellar rods; dorsal flagellum slightly protruding beyond flagellar pocket; fast gliding on surfaces; extrusomes absent. In swimming stage: cell bodies 10.6 to 11.4 μm ($11 \pm 0.3 \mu\text{m}$; $N = 4$) long and 3.6 to 3.8 μm ($3.7 \pm 0.1 \mu\text{m}$; $N = 4$) wide; flagella 2 to 2.5 of body length, with heteromorphic PFR; dorsal flagellum one third longer than ventral flagellum; fast swimming mediated by dorsal flagellum forming anterior loop and ventral flagellum loosely twisted along body; gradual transition from trophic to swimming stage.

Etymology: *aflagellata*, the species name describes the lack of long flagella in trophic stage; adjective.

Type strain: *Lacrimia aflagellata* Mex301.

Type material: hapantotype is a block of resin-embedded cells for transmission electron microscopy deposited in the protozoological collection of the Institute of Parasitology, Biology Centre, Czech Academy of Sciences, České Budějovice, Czech Republic under no. IPCAS Pro 84.

Gene sequence: NCBI acc. n. PP719295.

Type locality: seawater aquarium at the Zoo Payo Obispo, Chetumal, Mexico.

ZooBank: E6E17E30-77FF-4C65-8C11-BB45BF6DC3F7.

Phylum: Euglenozoa Cavalier-Smith, 1981.

Class: Diplonemea Cavalier-Smith, 1993.

Family: Diplonemidae Cavalier-Smith, 1993.

4.1.5. Genus *Natarhynchopus* Tashyreva, Horák et Lukeš, gen. n

Monospecific genus established based on the high molecular divergence of 18S rRNA gene from representatives of the genus *Rhynchopus* (~ 85 % identity) and morphological differences. Distinguished from *Rhynchopus* spp. by smaller size, considerably flattened bodies, fast gliding on surfaces, and frequent differentiation into swimming stage following starvation.

Etymology: from Latin *natāns*, meaning “swimming, floating”, describes the common transition to the fast-swimming stage under nutrient starvation.

Type species: *Rhynchopus humris* Tashyreva, Prokopchuk, Horák et Lukeš, 2018, here designated as *Natarhynchopus humris* comb. nov.

ZooBank: ADD09254-66 EB-4630-833F-36191CCB77F4.

4.2. Bacterial endosymbiont

Class: Alphaproteobacteria Garrity, 2006.

Order: Rhodospirillales Pfennig et Trüper, 1971.

Family: Holosporaceae Görtz et Schmidt, 2005.

Genus: *Cytomitobacter* Tashyreva, Prokopchuk et Lukeš, 2018.

4.2.1. “*Candidatus Cytomitobacter rhynchopi*” Tashyreva, Horák et Lukeš, sp. n

Description: intracellular symbiont of *Rhynchopus asiaticus* sp. n. isolate YZ270 clone 10 in abundances of 8 to 37 cells (20.7 ± 5.9 ; $N = 100$); designated as new species based on differences in 16S rRNA gene sequences from *Ca. Cytomitobacter primus* Tashyreva, Prokopchuk et Lukeš, 2018 and *Ca. Cytomitobacter indipagum* Tashyreva, Prokopchuk et Lukeš, 2018 (93.7 and 92 % identity, respectively); short rods ~0.9 μm long and ~0.45 μm wide; solitary cells randomly spread across host cytoplasm, not preferentially associated with any intracellular structures; infectious stages not detected.

Etymology: *rhynchopi*, the species name refers to the specific host.

Type host: *Rhynchopus asiaticus* YZ270 clone10.

Type material: a block of resin-embedded cells for transmission electron microscopy and ethanol-fixed host cells are deposited in the protozoological collection of the Institute of Parasitology, Biology Centre, under no. IPCAS Pro 85.

Gene sequence: full-length 16S rRNA gene sequence deposited in

GenBank under accession number PP719300.

CRediT authorship contribution statement

Daria Tashyreva: Writing – review & editing, Writing – original draft, Visualization, Methodology, Investigation, Funding acquisition, Conceptualization. **Jan Votýpka:** Writing – review & editing, Investigation. **Akinori Yabuki:** Writing – review & editing, Resources, Methodology. **Aleš Horák:** Writing – review & editing, Resources, Investigation, Funding acquisition. **Julius Lukeš:** Writing – review & editing, Resources, Funding acquisition, Conceptualization.

Declaration of competing interest

The authors declare that they have no known competing financial interests or personal relationships that could have appeared to influence the work reported in this paper.

Acknowledgements

This work was supported by grants from the Czech Grant Agency (23-06479× to JL and 21-26209S to AH), the Gordon and Betty Moore Foundation (#9354 to JL), and Polonez BIS 3 National Science Centre (UMO-2022/47/P/NZ8/02074 to DT). We thank Michael Hammond for the English editing of the manuscript.

All authors have seen and approved the final version of the manuscript being submitted. The authors confirm that the article is the authors’ original work, hasn’t received prior publication and isn’t under consideration for publication elsewhere.

The authors declare no conflict of interests.

Appendix A. Supplementary Data

Supplementary data to this article can be found online at <https://doi.org/10.1016/j.protis.2025.126090>.

References

- Benz, C., Raas, M.W.D., Tripathi, P., Faktorová, D., Tromer, E.C., Akiyoshi, B., Lukeš, J., 2024. On the possibility of yet a third kinetochore system in the protist phylum Euglenozoa. *mBio* 15, e02936–24. <https://doi.org/10.1128/mbio.02936-24>.
- Bodammer, J.E., Sawyer, T.K., 1981. Aufwuchs protozoa and bacteria on the gills of the rock crab, *Cancer irroratus* say: a survey by light and electron microscopy. *J. Protozool.* 28, 35–46. <https://doi.org/10.1111/j.1550-7408.1981.tb02801.x>.
- Bolger, A.M., Lohse, M., Usadel, B., 2014. Trimmomatic: a flexible trimmer for Illumina sequence data. *Bioinformatics* 30 (15), 2114–2120. <https://doi.org/10.1093/bioinformatics/btu170>.
- Cadena, L.R., Edgcomb, V., Lukeš, J., 2024. Gazing into the abyss: a glimpse into the diversity, distribution, and behaviour of heterotrophic protists from the deep-sea floor. *Environ. Microbiol.* 26, e16598. <https://doi.org/10.1111/1462-2920.16598>.
- de Vargas, C., Audic, S., Henry, N., Decelle, J., Mahé, F., Logares, R., Lara, E., Berney, C., Le Bescot, N., Probert, I., Carmichael, M., Poulain, J., Romac, S., Colin, S., Aury, J.-M., Bittner, L., Chaffron, S., Dunthorn, M., Engelen, S., Flegontova, O., Guidi, L., Horák, A., Jaillon, O., Lima-Mendez, G., Lukeš, J., Malviya, S., Morard, R., Mulot, M., Scalco, E., Siano, R., Vincent, F., Zingone, A., Dimier, C., Picheral, M., Searson, S., Kandels-Lewis, S., Acinas, S.G., Bork, P., Bowler, C., Gorsky, G., Grimsley, N., Hingamp, P., Iudicone, D., Not, F., Ogata, H., Pesant, S., Raes, J., Sieracki, M.E., Speich, S., Stemmann, L., Sunagawa, S., Weissenbach, J., Wincker, P., Karsenti, E., Boss, E., Follows, M., Karp-Boss, L., Krzic, U., Reynaud, E.G., Sardet, C., Sullivan, M.B., Velayoudon, D., 2015. Eukaryotic plankton diversity in the sunlit ocean. *Science* 348, 1261–1265. <https://doi.org/10.1126/science.1261605>.
- Faktorová, D., Kaur, B., Valach, M., Graf, L., Benz, C., Burger, G., Lukeš, J., 2020a. Targeted integration by homologous recombination enables *in situ* tagging and replacement of genes in the marine microeukaryote *Diplonema papillatum*. *Environ. Microbiol.* 22, 3660–3670. <https://doi.org/10.1111/1462-2920.15130>.
- Faktorová, D., Nisbet, R.E.R., Fernández Robledo, J.A., Casacuberta, E., Sudek, L., Allen, A.E., Ares, M., Aresté, C., Balestreri, C., Barbrook, A.C., Beardslee, P., Bender, S., Booth, D.S., Bouget, F.-Y., Bowler, C., Breglia, S.A., Brownlee, C., Burger, G., Cerutti, H., Cesaroni, R., Chiurillo, M.A., Clemente, T., Coles, D.B., Collier, J.L., Cooney, E.C., Coyne, K., Docampo, R., Dupont, C.L., Edgcomb, V., Einarsson, E., Elustondo, P.A., Federici, F., Freire-Beneítez, V., Freyria, N.J., Fukuda, K., García, P.A., Girguis, P.R., Goma, F., Gornik, S.G., Guo, J., Hampl, V., Hanawa, Y., Haro-Contreras, E.R., Hehenberger, E., Highfield, A., Hirakawa, Y., Hopes, A., Howe, C.J., Hu, I., Ibañez, J., Irwin, N.A.T., Ishii, Y., Janowicz, N.E.,

- Jones, A.C., Kachale, A., Fujimura-Kamada, K., Kaur, B., Kaye, J.Z., Kazana, E., Keeling, P.J., King, N., Klobutcher, L.A., Lander, N., Lassadi, I., Li, Z., Lin, S., Lozano, J.-C., Luan, F., Maruyama, S., Matute, T., Miceli, C., Minagawa, J., Moosburner, M., Najle, S.R., Nanjappa, D., Nimmo, I.C., Noble, L., Novák Vanclová, A.M.G., Nowacki, M., Nuñez, I., Pain, A., Piersanti, A., Pucciarelli, S., Pyrih, J., Rest, J.S., Rius, M., Robertson, D., Ruaud, A., Ruiz-Trillo, I., Sigg, M.A., Silver, P.A., Slamovits, C.H., Jason Smith, G., Sprecher, B.N., Stern, R., Swart, E.C., Tsaousis, A.D., Tsy-pin, L., Turkewitz, A., Turnšek, J., Valach, M., Vergé, V., von Dassow, P., von der Haar, T., Waller, R.F., Wang, L., Wen, X., Wheeler, G., Woods, A., Zhang, H., Mock, T., Worden, A.Z., Lukeš, J., 2020b. Genetic tool development in marine protists: emerging model organisms for experimental cell biology. *Nat. Methods* 17, 481–494. <https://doi.org/10.1038/s41592-020-0796-x>.
- Faktorová, D., Záhonová, K., Benz, C., Dacks, J.B., Field, M.C., Lukeš, J., 2023. Functional differentiation of Sec13 paralogs in the euglenozoan protists. *Open Biol.* 13, 220364. <https://doi.org/10.1098/rsob.220364>.
- Flegontova, O., Flegontov, P., Malviya, S., Audic, S., Wincker, P., de Vargas, C., Bowler, C., Lukeš, J., Horák, A., 2016. Extreme diversity of diplomonid eukaryotes in the ocean. *Curr. Biol.* 26, 3060–3065. <https://doi.org/10.1016/j.cub.2016.09.031>.
- Flegontova, O., Flegontov, P., Londoño, P.A.C., Walczowski, W., Santic, D., Edgcomb, V. P., Lukeš, J., Horák, A., 2020. Environmental determinants of the distribution of planktonic diplomonids and kinetoplastids in the oceans. *Environ. Microbiol.* 22 (9), 4014–4031. <https://doi.org/10.1111/1462-2920.15190>.
- Flegontova, O., Lukeš, J., Horák, A., 2023. Intragenomic diversity of the V9 hypervariable domain in eukaryotes has little effect on metabarcoding. *iScience* 26 (8), 107291. <https://doi.org/10.1016/j.isci.2023.107291>.
- Gawryluk, R.M.R., del Campo, J., Okamoto, N., Strasser, J.F.H., Lukeš, J., Richards, T. A., Worden, A.Z., Santoro, A.E., Keeling, P.J., 2016. Morphological identification and single-cell genomics of marine diplomonids. *Curr. Biol.* 26, 3053–3059. <https://doi.org/10.1016/j.cub.2016.09.013>.
- George, E.E., Husnik, F., Tashyreva, D., Prokopcuk, G., Horák, A., Kwong, W.K., Lukeš, J., Keeling, P.J., 2020. Highly reduced genomes of protist endosymbionts show evolutionary convergence. *Curr. Biol.* 30, 925–933.e3. <https://doi.org/10.1016/j.cub.2019.12.070>.
- Giovannini, M., Petroni, G., Castelli, M., 2024. Novel evolutionary insights on the interactions of the Holosporales (Alphaproteobacteria) with eukaryotic hosts from comparative genomics. *Environ. Microbiol.* 26 (1), e16562. <https://doi.org/10.1111/1462-2920.16562>.
- Görtz, H., Schmidt, H.J., 2015. Holosporaceae fam. Nov., in: Bergey's Manual of Systematics of Archaea and Bacteria. Wiley, pp. 1–6. <https://doi.org/10.1002/9781118960608.fbm00177>.
- Gouy, M., Tannier, E., Comte, N., Parsons, D.P., 2021. Seaview Version 5: a multiplatform software for multiple sequence alignment, molecular phylogenetic analyses, and tree reconciliation. *Methods Mol. Biol.* 2231, 241–260. https://doi.org/10.1007/978-1-0716-1036-7_15.
- Israelsson, O., 2007. Chlamydial symbionts in the enigmatic *Xenoturbella* (Deuterostomia). *J. Invertebr. Pathol.* 96, 213–220. <https://doi.org/10.1016/j.jip.2007.05.002>.
- Katoh, K., Standley, D.M., 2013. MAFFT multiple sequence alignment software version 7: improvements in performance and usability. *Mol. Biol. Evol.* 30, 772–780. <https://doi.org/10.1093/molbev/mst010>.
- Kaur, B., Záhonová, K., Valach, M., Faktorová, D., Prokopcuk, G., Burger, G., Lukeš, J., 2020. Gene fragmentation and RNA editing without borders: eccentric mitochondrial genomes of diplomonids. *Nucleic Acids Res.* 48, 2694–2708. <https://doi.org/10.1093/nar/gkz1215>.
- Kent, M.L., Elston, R.A., Nerad, T.A., Sawyer, T.K., 1987. An *Isonema*-like flagellate (Protozoa: Mastigophora) infection in larval geoduck clams, *Panope abrupta*. *J. Invertebr. Pathol.* 50, 221–229.
- Kim, M., Oh, H.-S., Park, S.-C., Chun, J., 2014. Towards a taxonomic coherence between average nucleotide identity and 16S rRNA gene sequence similarity for species demarcation of prokaryotes. *Int. J. Syst. Evol. Microbiol.* 64, 346–351. <https://doi.org/10.1099/ijs.0.059774-0>.
- Kostygov, A.Y., Karnkowska, A., Votýpka, J., Tashyreva, D., Maciszewski, K., Yurchenko, V., Lukeš, J., 2021. Euglenozoa: taxonomy, diversity and ecology, symbioses and viruses. *Open Biol.* 11, 200407. <https://doi.org/10.1098/rsob.200407>.
- Lartillot, N., Lepage, T., Blanquart, S., 2009. PhyloBayes 3: a Bayesian software package for phylogenetic reconstruction and molecular dating. *Bioinformatics* 25, 2286–2288. <https://doi.org/10.1093/bioinformatics/btp368>.
- Lax, G., Okamoto, N., Keeling, P.J., 2024. Phylogenomic position of eupelagomids, abundant, and diverse deep-ocean heterotrophs. *ISME J.* 18 (1), wrae040. <https://doi.org/10.1093/ismej/jwae040>.
- Liu, L., Wang, Y., Yang, Y., Wang, D., Cheng, S.H., Zheng, C., Zhang, T., 2021. Charting the complexity of the activated sludge microbiome through a hybrid sequencing strategy. *Microbiome* 9, 205. <https://doi.org/10.1186/s40168-021-01155-1>.
- Lukeš, J., Čepička, I., Kolísko, M., 2024. Evolution: no end in sight for novel incredible (heterotrophic) protists. *Curr. Biol.* 34, R55–R58. <https://doi.org/10.1016/j.cub.2023.10.065>.
- Maslov, D.A., Ziková, A., Kyselová, I., Lukeš, J., 2002. A putative novel nuclear-encoded subunit of the cytochrome c oxidase complex in trypanosomatids. *Mol. Biochem. Parasitol.* 125, 113–125. [https://doi.org/10.1016/S0166-6851\(02\)00235-9](https://doi.org/10.1016/S0166-6851(02)00235-9).
- Minh, B.Q., Schmidt, H.A., Chernomor, O., Schrempf, D., Woodhams, M.D., von Haeseler, A., Lanfear, R., 2020. IQ-TREE 2: New models and efficient methods for phylogenetic inference in the genomic era. *Mol. Biol. Evol.* 37, 1530–1534. <https://doi.org/10.1093/molbev/msaa015>.
- Montegut-Felkner, A.E., Triemer, R.E., 1996. Phylogeny of *Diplonema ambulator* (Larsen and Patterson). *Eur. J. Protistol.* 32, 64–76. [https://doi.org/10.1016/S0932-4739\(96\)80040-X](https://doi.org/10.1016/S0932-4739(96)80040-X).
- Mukherjee, I., Hodoki, Y., Okazaki, Y., Fujinaga, S., Ohbayashi, K., Nakano, S., 2019. Widespread dominance of kinetoplastids and unexpected presence of diplomonids in deep freshwater lakes. *Front. Microbiol.* 10, 2375. <https://doi.org/10.3389/fmicb.2019.02375>.
- Muñoz-Gómez, S.A., Hess, S., Burger, G., Lang, B.F., Susko, E., Slamovits, C.H., Roger, A. J., 2019. An updated phylogeny of the Alphaproteobacteria reveals that the parasitic Rickettsiales and Holosporales have independent origins. *eLife* 25 (8), e42535. <https://doi.org/10.7554/eLife.42535>.
- Nerad, T., 1990. The Life History, Cytology and Taxonomy of *Isonema* and *Isonema*-Like Flagellates. University of Maryland, College Park, MD (259 p Ph.D. Thesis.).
- Nylund, S., Steigen, A., Karlsbakk, E., Plarre, H., Andersen, L., Karlsen, M., Watanabe, K., Nylund, A., 2015. Characterization of 'Candidatus Syngnamydia salmonis' (Chlamydiales, Simkaniaceae), a bacterium associated with epitheliocystis in Atlantic salmon (*Salmo salar* L.). *Arch. Microbiol.* 197, 17–25. <https://doi.org/10.1007/s00203-014-1038-3>.
- Nylund, A., Pistone, D., Trösse, C., Blindheim, S., Andersen, L., Plarre, H., 2018. Genotyping of *Candidatus Syngnamydia salmonis* (Chlamydiales: Simkaniaceae) co-cultured in *Paramoeba perurans* (Amoebozoa: Paramoebidae). *Arch. Microbiol.* 200, 859–867. <https://doi.org/10.1007/s00203-018-1488-0>.
- Okamoto, N., Gawryluk, R.M.R., Campo, J., Strasser, J.F.H., Lukeš, J., Richards, T.A., Worden, A.Z., Santoro, A.E., Keeling, P.J., 2019. A revised taxonomy of diplomonids including the Eupelagomidae n. fam. And a type species, *Eupelagomena oceanica* n. gen. & sp. *J. Eukaryot. Microbiol.* 66, 519–524. <https://doi.org/10.1111/jeu.12679>.
- Pilatová, J., Tashyreva, D., Týč, J., Vancová, M., Bokhari, S.N.H., Skoupý, R., Klementová, M., Kúpper, H., Mojžes, P., Lukeš, J., 2023. Massive accumulation of strontium and barium in diplomonid protists. *mBio* 14. <https://doi.org/10.1128/mbio.03279-22> e03279–22.
- Pillonel, T., Bertelli, C., Salamin, N., Greub, G., 2015. Taxogenomics of the order Chlamydiales. *Int. J. Syst. Evol. Microbiol.* 65, 1381–1393. <https://doi.org/10.1099/ijs.0.000090>.
- Prjibelski, A., Antipov, D., Meleshko, D., Lapidus, A., Korobeynikov, A., 2020. Using SPAdes de novo assembler. *Curr. Protoc. Bioinformatics*, 70, e102. Doi: 10.1002/cpbi.102Roy, J., Faktorová, D., Benada, O., Lukeš, J., Burger, G., 2007. Description of *Rhynchopoe euleides* n. sp. (Diplonemea), a free-living marine euglenozoan. *J. Eukaryot. Microbiol.* 54, 137–145. <https://doi.org/10.1111/j.1550-7408.2007.00244.x>.
- Roy, J., Faktorová, D., Benada, O., Lukeš, J., Burger, G., 2007. Description of *Rhynchopoe euleides* n. sp. (Diplonemea), a free-living marine euglenozoan. *J. Eukaryot. Microbiol.* 54, 137–145. <https://doi.org/10.1111/j.1550-7408.2007.00244.x>.
- Schnepf, E., 1994. Light and electron microscopical observations in *Rhynchopoe coccinodiscivorus* spec. Nov., a colorless, phagotrophic euglenozoan with concealed flagella. *Arch. Protistenkunde* 144, 63–74. [https://doi.org/10.1016/S0003-9365\(11\)80225-3](https://doi.org/10.1016/S0003-9365(11)80225-3).
- Simpson, A.G.B., 1997. The identity and composition of the Euglenozoa. *Arch. Protistenkunde* 148, 318–328. [https://doi.org/10.1016/S0003-9365\(97\)80012-7](https://doi.org/10.1016/S0003-9365(97)80012-7).
- Skujaj, H., 1948. Taxonomie des Phytoplanktons einiger Seen in Uppland. Schweden. *Symb. Bot. Ups.* 9, 5–399.
- Tashyreva, D., Prokopcuk, G., Votýpka, J., Yabuki, A., Horák, A., Lukeš, J., 2018a. Life cycle, ultrastructure, and phylogeny of new diplomonids and their endosymbiotic bacteria. *mBio* 9. <https://doi.org/10.1128/mBio.02447-17> e02447–17.
- Tashyreva, D., Prokopcuk, G., Yabuki, A., Kaur, B., Faktorová, D., Votýpka, J., Kusaka, C., Fujikura, K., Shiratori, T., Ishida, K.-I., Horák, A., Lukeš, J., 2018b. Phylogeny and morphology of new diplomonids from Japan. *Protist* 169, 158–179. <https://doi.org/10.1016/j.protis.2018.02.001>.
- Tashyreva, D., Simpson, A.G.B., Prokopcuk, G., Škodová-Sveráková, I., Butenko, A., Hammond, M., George, E.E., Flegontova, O., Záhonová, K., Faktorová, D., Yabuki, A., Horák, A., Keeling, P.J., Lukeš, J., 2022. Diplomonids – a review on “new” flagellates on the oceanic block. *Protist* 173, 125868. <https://doi.org/10.1016/j.protis.2022.125868>.
- Tashyreva, D., Týč, J., Horák, A., Lukeš, J., 2023. Ultrastructure and 3D reconstruction of a diplomonid protist (Diplonemea) and its novel membranous organelle. *mBio* 14. <https://doi.org/10.1128/mbio.01921-23> e01921–23.
- Valach, M., Benz, C., Aguilar, L.C., Gahura, O., Faktorová, D., Ziková, A., Oeffinger, M., Burger, G., Gray, M.W., Lukeš, J., 2023a. Miniature RNAs are embedded in an exceptionally protein-rich mitoribosome via an elaborate assembly pathway. *Nucleic Acids Res.* 51, 6443–6460. <https://doi.org/10.1093/nar/gkad422>.
- Valach, M., Moreira, S., Petitjean, C., Benz, C., Butenko, A., Flegontova, O., Nenarokova, A., Prokopcuk, G., Batstone, T., Lapébie, P., Lemogo, L., Sarasin, M., Stretenowich, P., Tripathi, P., Yazaki, E., Nara, T., Henrissat, B., Lang, B.F., Gray, M. W., Williams, T.A., Lukeš, J., Burger, G., 2023b. Recent expansion of metabolic versatility in *Diplonema papillatum*, the model species of a highly speciose group of marine eukaryotes. *BMC Biol.* 21, 99. <https://doi.org/10.1186/s12915-023-01563-9>.
- Viver, T., Orellana, L.H., Hatt, J.K., Urdiain, M., Díaz, S., Richter, M., Antón, J., Avian, M., Amann, R., Konstantinidis, K.T., Rosselló-Móra, R., 2017. The low diverse gastric microbiome of the jellyfish *Cotylorhiza tuberculata* is dominated by four novel taxa. *Environ. Microbiol.* 19, 3039–3058. <https://doi.org/10.1111/1462-2920.13763>.
- von der Heyden, S., Chao, E.E., Vickerman, K., Cavalier-Smith, T., 2004. Ribosomal RNA phylogeny of bodonid and diplomonid flagellates and the evolution of Euglenozoa. *J. Eukaryot. Microbiol.* 51, 402–416. <https://doi.org/10.1111/j.1550-7408.2004.tb00387.x>.